Transient and thermo-economic analysis of MED-MVC desalination process

Mohamed L. Elsayed [a,b,1], Osama Mesalhy [a,b], Ramy H. Mohammed [a,b], Louis C. Chow [a]
[a]Department of Mechanical and Aerospace Engineering, University of Central Florida, Orlando, FL 32816-2450, USA.
[b]Department of Mechanical Power Engineering, Zagazig University, Zagazig 44519, Egypt.

ABSTRACT

An exergo-economic model is used to assess the performance of a multi-effect desalination plant integrated to a mechanical vapor compressor unit (MED-MVC) with a water production capacity of 1500 m^3/day. The results show that the second law efficiency (η_{II}) is 2.8%. The MVC and evaporator units are responsible for about 39 and 52% of the total exergy destruction, respectively. The total water price (TWP) is 1.70 \$/m^3 when calculated using a simple conventional economic model and 1.63 \$/m^3 when calculated using an exergy-based cost model. Increasing the number of effects from 1 to 6 results in a 39% reduction in the specific power consumption (SPC), a 70% increase in η_{II} and a 24% decrease in TWP. A dynamic model is developed to investigate the effect of fluctuations of compressor work ($\dot{W}_c$) and inlet seawater temperature (T_{sw}) on the plant behavior and performance. The dynamic model results show that the disturbance in $\dot{W}_c$ has a significant effect on the plant transient behavior and may cause the plant to cease operation while a disturbance in T_{sw} has only a moderate impact. Increasing T_{sw} above a certain value of the steady-state condition without proper control on the plant response could lead to evaporator dry out. In term of performance, a reduction in $\dot{W}_c$ causes a decrease in the plant production capacity and SPC, while it increases the plant performance ratio (PR). On the other hand, a reduction in the inlet T_{sw} causes a reduction in the plant production capacity and PR and an increase in SPC for the same compressor work. Furthermore, a comparison between a MED-MVC system and a MED integrated to a thermal vapor compressor system (MED-TVC) reveals that the latter system is rather sensitive to the reduction in T_{sw} due to the presence of the condenser unit in the MED-TVC. The response of the MED-MVC system is slower than the MED-TVC which is due to the high thermal capacity of the preheaters for the feed in the MED-MVC.

KEYWORDS: Seawater; Cost diagram; Mechanical vapor compression (MVC); Dynamic disturbance.

[1]E-mail: mlea@knights.ucf.edu, mlabdelkrem@zu.edu.eg (Mohamed L. Elsayed).

Introduction

Seawater desalination is considered a viable solution for drinking water shortage besides other integrated solutions such as water management, reclamation and better water conservation. There are two primary desalination techniques: membrane (non-thermal) and evaporation (thermal) processes. Membrane techniques such as reverse osmosis (RO) are characterized by low energy consumption but also low water product quality associated with residuals of borides, chlorides and bromides, as well as high maintenance cost and short membrane lifespan [1]. Thermally-driven processes such as Multi-Effect Desalination (MED), Multi-Stage Flash Desalination (MSF), Mechanical and Thermal Vapor Compression (MVC and TVC) are usually used in countries such as Gulf co-operation countries (GCC) where the supplied feed seawater is exhibited to changes in feed quality arising from fine sand, silt, harmful algae blooms (HABs) and water salinity fluctuation [2]. Recovering the latent heat of condensation in the product vapor was proposed through heat pump concepts such as TVC and MVC units to allow further evaporation of seawater when the temperature level of the produced vapor is too low for stable evaporation. The MVC evaporation system has been widely studied and frequently applied as a solution for medium-scale (100-4000 m^3/day) water reclamation desalination and solution concentration for high-salinity wastewater treatment (salt recovery) [3]. The advantages associated with MVC systems are high-quality water recovered that need little or no treatment, compact equipment, low operating cost, stable operation and simple integration with renewable energy systems [4]. The low capacity of available vapor compressors, low volumetric flow and low-pressure head limit the production capacity of MED-MVC systems to 5000 m^3/day [5].

Various studies for MVC systems are available in the literature and include steady-state mathematical model development, simplified design methods, experimental research and performance prediction. For instance, Helal and Al-Malek [6] presented a hybrid diesel/solar photovoltaic (PV) assisted MVC desalination system. The system was to supply small communities in remote areas with drinkable water

at a production capacity of 120 m^3/day. A diesel engine was used to overcome the uncertainty in the availability of solar energy. Henderson et al. [7] proposed a wind/diesel hybrid driven MVC desalination system for off electric grid locations in the USA. Optimization of a similar plant driven by wind/PV hybrid was carried out by Zejli et al. [8] for a water production capacity of 120 m^3/day. An energy storage system was used to store the extra power generated to address the intermittent nature of the renewable energy used.

Exergy analysis is known as a powerful tool to analyze the performance of mechanical and thermal systems. Using such method to analyze seawater desalination systems is a practical approach to identify the components with high thermodynamic irreversibilities [9]. Such information is useful to show which components in the system have room for improvement to increase the overall exergy efficiency and to optimize designs [10]. Alasfour and Abdulrahim [11] applied a steady-state model using the second law of thermodynamics to a single-effect MVC unit. The results indicated that an increase in the temperature drop across the effect causes an increase in exergy destruction. Nafey et al. [12] analyzed a MED-MVC system with a two-effect forward-feed configuration plant and showed that the specific power consumption (SPC), second law exergetic efficiency (η_{II}) and the unit product cost are 9.4 kWh/m^3, 5.7% and 1.7 \$/ m^3, respectively. Ahmadi et al. [13] compared a single- and two-effect mechanical vapor recompression (MVR) and showed that energy saving can be achieved by using the two-effect MVR rather than the single-effect one. Also, the reduction in heat transfer area was 5.6 m^2 for the two-effect system compared to the single-effect one.

Recently, MED-MVC systems have been used as brine concentrators before sending the brine to crystallizers or evaporation ponds. These system combinations are called Zero liquid discharge (ZLD) systems [14]. Typically, the crystallizers have a constant evaporation capacity. Thus the evaporator rejected brine mass or content should be controlled to maintain the optimum operational conditions, leading to energy savings and prevention of scale formation. Therefore, the system transient behavior

needs to be predicted to conduct control strategies, examine different scenarios of operation, handle the possibility of unexpected transient conditions, and guarantee a relatively stable output through the production duration [15].

Thermal desalination systems may be exposed to unexpected fluctuations (disturbances) in input parameters throughout their operation periods that include environmental changes such as swings in the feed seawater temperature due to varying weather condition and swings in the supplied heat source. The second type of fluctuations is called "turndown" that represents the possible change in total plant output. This type of disturbance is carried out by design to address a swing in the power requirement [16]. Dynamic simulation can predict the system behavior from start up to shut down and can be used to establish advanced control strategies and test operating scenarios. It can also address potential problems related to unexpected transient events, and produce a comparatively stable output during the production period [17]. Several efforts were made to study the dynamic characteristics of conventional thermal desalination MED [18-21] and MED-TVC systems [22-25]. For instance, at CIEMAT-Plataforma Solar de Almerı´a (PSA), a transient operation model of the MED plant in a vertical arrangement was developed and solved using the object-oriented Modelica language [19]. The model was divided into sub-models that encapsulated and covered the dynamics of each one of the sub-processes that took place in the system in order to study the plant performance in different scenarios and design operating strategies to improve its efficiency [20]. Furthermore, Roca et al. [21] developed a dynamic model using Modelica for MED systems and the results were validated using data from the PSA facility. Two first-order models for the distillate production and outlet MED temperature as a function of inlet MED temperature were obtained by linearizing the dynamic model in [20] and good agreement was obtained for a wide operation range. For MED-TVC systems, Mazini et al. [23] developed a lumped dynamic model and validated it with actual data from a MED-TVC operating plant. Although disturbances in feed flow rate and seawater temperature were considered, the physics of the system response was not clearly illustrated. Cipollina et

al. [24] used the gPROMS® dynamic simulator to predict the transient behavior of a MED-TVC based on available data from the Trapani plant in Italy. The dynamic operation was obtained by applying changes to specific disturbances on the main input parameters. Negligible variations were predicted with an increase in the seawater temperature, while a slight reduction in the plant gain output ratio (GOR= distillate to steam supplied ratio) was shown when the seawater temperature was reduced. Recently, a comprehensive model was developed by Elsayed et al. [25] to study the dynamic characteristics of different feed configurations of MED systems and MED-TVC as well. The simulation results revealed that MED-TVC with parallel/cross feed has the fastest response compared to slower response associated with backward and forward feed for the same applied disturbances. Furthermore, the MED-TVC is more susceptible to the heat sink disturbances compared to the other traditional MED configurations.

There have been very few efforts to model the dynamic nature of the MVC evaporation systems. For instance, El-Khatib et al. [26] proposed a transient model through control of multiple inputs and outputs to an MVC single-effect desalination unit. The model is limited to the dynamic representation of the vapor temperature inside the effect without considering the level of the brine pool or the brine salinity. Two changes were applied to the MVC unit, namely a variation in the production of distillate flow rate and the inlet feed flow rate of ±20 %. The model results were not validated by experimental or actual operating data. Kishore et al. [27] proposed a dynamic simulator for the MED-MVC system as work-in-progress for steady state and the dynamic behaviors. However, no system response due to load change was shown. Another contribution in dynamic simulation and control for a single-effect MVC to investigate the acceptable level of parameter disturbances in the dairy industry was made by Winchester and Marsh [28]. It is essential to study the dynamic behavior of a MED-MVC system subject to changes in the input operating parameters to improve the understanding of the process behavior and performance. In the present study, a dynamic model to study the transient behavior of a parallel/cross feed MED-MVC desalination system is developed based on the work on MED-TVC reported by Elsayed et al. [25] by

adding features that are in the MED-MVC but not in the MED-TVC. The present model is also modified and customized with equations that dynamically track the behavior of four effects, two preheaters and a mechanical compressor unit. Three nonlinear ordinary differential equations are derived for three state variables, namely the vapor temperature, brine salinity and brine level, to simulate the dynamics of the evaporator effect. Also, a dynamic model for the brine and distillate preheaters is developed to obtain the transient variation of the inlet and outlet stream temperatures. Finally, the entire set of equations is solved simultaneously using the Runge-Kutta fourth-order. The dynamic model yields the plant behavior and performance under various fluctuations in the main input operating conditions that include the compressor work and inlet seawater temperature. Furthermore, the exergo-economic analysis is used to assess the MED-MVC system performance and to obtain the total water price compared to the simple conventional economic method.

MED-MVC process description

A parallel/cross feed (PCF) multi-effect-desalination integrated with a mechanical vapor compression unit is considered in the present study. A schematic diagram of MED-MVC is shown in Fig. 1. A typical MED-MVC system contains major elements such as a train of horizontal falling film evaporators, MVC unit, pre-heaters for intake seawater, a boiler which supplies the external steam, pumps for brine and product, a venting system to remove non-condensable gases, along with an operating control system [29]. Each evaporator consists of a shell that houses tube bundles of horizontal falling film tubes, spray nozzles, demister and space for the vapor and brine pool. Vapor compression is a cyclic process [30], so the entire vapor generated in the last effect is routed through a wire mesh mist eliminator (demister) to separate water droplets from the vapor before entering the compressor. The vapor is compressed to the desired target temperature and pressure before directing it as supply steam to the inside of the 1^{st} effect tube bundles. The supply steam from the MVC unit condenses inside the tube bundles by rejecting its latent heat to the continuously sprayed thin film of the seawater feed on the exterior wall of the tube

bundles. The temperature of the feed seawater around the tubes in the 1st effect is raised to its saturation temperature that is known as top brine temperature (TBT). Part of the supplied seawater feed to the 1st effect vaporizes, and the vapor flows into the 2nd effect which is at a lower pressure and temperature than the first effect. The evaporated portion of the feed in each effect works as a heat source for the following effect. In all effects, condensation and evaporation occur simultaneously inside and outside the tubes for vapor and thin sprayed seawater film, respectively. The unevaporated portion of the supplied seawater feed (brine) from the first effect flows into the second effect to utilize its energy by flashing due to the abrupt decrease in pressure when the brine leaves the first effect and enters the second effect. The brine continues to flow through all effects until it finally reaches the last effect as shown in Fig. 1. The vapor inside the 2nd to the last effect is produced by both evaporation and flashing. The concentrated brine and fresh water produced are drawn to the preheaters by pumps at a temperature above the ambient temperature.

In the MED-MVC system, there is no need for a condenser as in conventional MED systems, but two multi-flow plate-type heat exchangers (pre-heaters) are needed to recuperate the heat from both the product and brine blowdown streams. The feed seawater is split into two streams, and its temperature is elevated by passing through the pre-heaters. The supplied feed seawater is divided and directed into a series of consecutively lower pressure effects. The supplied feed is atomized and directed to the outside walls of the horizontally installed tubes forming a thin liquid film. Industrial MED-MVC desalination plants operate at temperatures between about 50-70°C. At such low temperature, the conditions favoring the deposition of insoluble sulfates and carbonates do not exist [31], and the risk of material corrosion is minimal.

Electricity is the only required source to operate the MED-MVC system. However, for start-up purpose and maintaining normal operating conditions without compressor surge, external steam (make-up steam) obtained from a steam boiler or extracted from a steam turbine may be needed to raise the 1st effect

temperature to the TBT [32, 33]. The mechanical energy required for a MED-MVC desalination system can be provided through the energy produced by a steam power plant (mechanically shaft driven). Also, electricity-driven MVC can be used by drawing electrical power from the electricity grid or a renewable energy source, or electrical energy generator if electricity services are not available. It has been demonstrated that the use of a MED-MVC system coupled with an electrical power generator is suitable for use in remote locations where water transport is expensive [8]. Energy is needed to activate the MVC unit, pumps, vacuum system and other control components. It is worth noting that the MVC unit represents the main power consuming component in MED-MVC system [11]. This power required depends on the vapor compression ratio, the thermodynamic efficiency of the polytropic process and the efficiency of the electric motor if one is used. For the MED-MVC system, the SPC (kWh/m^3) is represented in terms of the enthalpy difference of the compressed vapor (supply steam) and the inlet vapor from the last effect.

Models development

a. Steady-state model

The steady-state conservation equations of mass, energy, and salt are solved to obtain the steady-state values of all the parameters in the plant. The assumptions used in the steady-state model for a MED-MVC system are listed as follows:

1. Since the presence of non-condensable gases is normally vented out of the MED system whenever needed, the effect of non-condensable gases on evaporator performance is not considered.
2. Properties of the seawater brine and water vapor depend on temperature and salt content [34].
3. The temperature difference between the brine pool and vapor generated in an effect is due to the following reasons; (i) boiling point elevation (BPE), and (ii) non-equilibrium allowance (NEA).
4. The vapor and produced freshwater are salt-free.

Using the above assumptions, the steady-state mass, energy and salt balance equations for a MED-MVC system are obtained and presented in Table 1.

The isentropic work of the MVC unit is calculated from:

$$\dot{W}_{i,c} = \dot{m}_s \frac{\gamma . P_n . v_n}{(\gamma - 1)} \left(\left(\frac{P_s}{P_n} \right)^{\frac{\gamma - 1}{\gamma}} - 1 \right) \quad (1)$$

where γ is the specific heats ratio, P_s is the pressure at the compressor outlet which is the saturation pressure at the steam inlet temperature T_s, P_n is the pressure at the compressor inlet, and v_n is the specific volume of the vapor from the last effect.

The energy supplied to the first effect as shown in Fig. 2 is defined as:

$$Q_{s,1} = \dot{m}_s . \lambda_s + E_{SH} \quad ; \quad E_{SH} = \dot{m}_s \left(h_{v,\acute{T}_s} - h_{v,T_s} \right) \quad (2)$$

where $\dot{m}_s . \lambda_s$ represents the heat of condensation at T_s of the vapor produced in the last effect and E_{SH} represents the rate of energy gained by compression above the saturation condition, $h_{v,\acute{T}_s}$ is the enthalpy of the superheated vapor at the compressor exit, and h_{v,T_s} is the saturation enthalpy of the compressed vapor. The actual compressor work can be calculated from:

$$\dot{W}_c = \dot{m}_s . \left(h_{v,\acute{T}_s} - h_{v,T_n} \right) \quad (3)$$

where h_{v,T_n} is the saturated vapor enthalpy at the compressor inlet.

The primary contributor to the SPC in a MED-MVC system is the compressor work which depends on the compressor efficiency, compression ratio and inlet vapor specific volume. The secondary consumptions are due to vacuum pumps and starting up the boiler [35]. The SPC is calculated by:

$$\mathrm{SPC}(kWh/\mathrm{m}^3) = \frac{\dot{W}_{\mathrm{compressor}} + \sum \dot{W}_{\mathrm{pumps}}}{\mathrm{D}\ (\mathrm{m}^3/h)} \quad (4)$$

The performance ratio (PR) is calculated by the following relation as suggested by Nafey [12] which is modified to accommodate the actual work converted to the primary fuel energy. For conventional fossil fuel-based power plant, Shahzad et al. suggested a thermal to work conversion factor less than 0.45 [36].

$$\mathrm{PR} = \frac{D\lambda_d}{\dot{m}_s.\lambda_s + \frac{\dot{W}_c}{\eta_{thermal}=0.35}} \tag{5}$$

Different modeling methods exist for the modeling of (chevron) plate heat exchangers. For design purposes, the thermal effectiveness method and the log-mean-temperature-difference (LMTD) method are often used to model the steady-state performance of a plate heat exchanger. In this regard, two multi-flow direction plate type heat exchangers with an effectiveness of 0.8 are used in the current simulation to preheat the seawater inlet feed. The total feed is divided into two portions: one portion flows into the brine heat exchanger and the second portion flows into the distillate heat exchanger. The heat transfer areas for both heat exchangers are calculated based on the log mean temperature differences and the estimated overall heat transfer coefficients for the plate type heat exchangers (U_B and U_D) using the following equations:

$$A_{b,HEx} = \frac{\dot{m}_B(h_{b,n}-h_{o,b})}{U_B.LMTD_{b,HEx}} \quad , \quad A_{d,HEx} = \frac{\dot{m}_D(h_{hin,d}-h_{o,d})}{U_D.LMTD_{d,HEx}} \tag{6}$$

The log mean temperature differences in the brine and distillate preheaters $LMTD_{HEx(B,D)}$ are calculated using the following equations:

$$LMTD_{b,HEx} = \frac{(T_{b,n}-T_{F,b})-(T_{o,b}-T_{cw})}{ln\left[\frac{T_{b,n}-T_{F,b}}{T_{o,b}-T_{sw}}\right]}, \; LMTD_{d,HEx} = \frac{(T_{hin,d}-T_{F,d})-(T_{o,d}-T_{cw})}{ln\left[\frac{T_{hin,d}-T_{F,d}}{T_{o,d}-T_{sw}}\right]} \tag{7}$$

The mixing temperature of the distillate from the plant ($T_{hin,d}$) is calculated by:

$$T_{hin,d} = \frac{\sum_{i=1}^{n-1} D_i \, c_{P[T_{v,i}]} T_{v,i} + D_n c_{P[T_s]} T_s}{D c_{P[T_{hin,d}]}} \tag{8}$$

The total heat transfer coefficient for the plate type heat exchangers is calculated using:

$$U_{B,D} = \left[\frac{1}{h_o} + \frac{1}{h_o} + R_{f,o} + R_{f,o} + \frac{\delta_{plate}}{k_{wall}}\right]^{-1} \quad (9)$$

where k_{wall} is the thermal conductivity of the stainless steel plates, and the inner/outer convective heat transfer coefficients (h_i, h_o) are obtained using the following correlation [37]:

$$h_{o,i} = 0.2536 Re^{0.65} Pr^{0.4} \left(\frac{k_{wall}}{D_{eq}}\right), Re = \frac{\rho V D_{eq}}{\mu}, D_{eq} = \frac{4(W.t_{plate})}{2(w+t_{plate})} \sim 2t_{plate} \quad (10)$$

where w is the plate width, δ_{plate} is the plate thickness and t_{plate} is the plate spacing. The velocity of each stream is V (m/s) and Re is the stream flow Reynolds number. The previous equation is valid for water in the following ranges: $Re > 400$, $1.5 < Pr < 5.0$ [37].

The second law exergetic efficiency for a MED-MVC system is the ratio of the exergy employed to change the salinity of the products (the minimum work of separation) to the total exergy consumed [38] and is calculated by:

$$\eta_{II} = 1 - \frac{\dot{E}_{D,total}}{\dot{E}_{in,total}} = \frac{\dot{W}_{min}}{\dot{E}_{in,total}} \quad (11)$$

where, $\dot{E}_{in,total}$ is the sum of the exergies at the various inlet fluid streams in addition to the exergies supplied to the compressor and pumps. $\dot{E}_{D,total}$ is the exergy consumption and can be expressed as the sum of the subsystem exergy destructions. $\dot{W}_{min}$ is the minimum work input for the salt separation for a certain amount of seawater feed from a state of 25°C, 1 atm and a salinity of 36 ppt to fresh water with zero salinity, while rejecting the saline water at the same temperature and pressure. For a steady flow adiabatic process this work is equal to the difference between the stream exergies at the outlets and inlet [10].

$$\dot{W}_{min} = \dot{E}_{o,b} + \dot{E}_{o,d} - \dot{E}_{sw} \quad (12)$$

where, $\dot{E}_{o,b}$ and $\dot{E}_{o,d}$ represent the exergy of the outlet brine and distillate, respectively, while $\dot{E}_{sw}$ represents the exergy of the inlet feed water stream.

b. Simple cost model.

The production cost is divided into direct/indirect costs and annual operating cost. The direct capital costs (DCCs) represent the costs that are directly associated with the desalination plant construction and the process components purchase [39]. Table 2 presents the equations used to estimate the price of the MED-MVC system components. The other direct costs (land, well construction, auxiliary equipment and building construction) are estimated to be ~80K $ following the approach given in [40] for a fixed production capacity (1500 m^3/day). The total DCC is equal to the summation of the purchased equipment for the MED-MVC system in Table 2 plus the other remaining costs. Also, the indirect capital cost IDCC (freight, insurance, construction overhead, owner's costs and contingency costs) is expressed as a percentage of the total direct capital cost and is estimated by IDCC = 0.15*DCC [40].

The operating costs include all expenses afforded after plant commissioning and during real operation and are classified as variable and fixed costs. The variable operating costs are those related to the price of electrical power, heat source, chemicals for pre/post-treatments and other requirements that depend on the plant production capacity and standards. The fixed operating costs are used for the plant operation and are related to the plant capacity or taken as a factor of the direct capital cost (DCC). A cost index from Marshall and Swift equipment chemical engineering plant cost index (PCI) is used to accommodate the equipment price change and to fit the current time calculations (year 2018) [41]. Since the compressor cost often presents the most considerable part of the MVC direct costs, a linearly dependent compressor cost of the compressor work is assumed based on the work done by Lukic et al. [40]. Both variable and fixed operating costs are obtained based on published data from the literature [34]. Also, maintenance costs are taken as a portion of the fixed operating cost. Investment and operating costs analyses are performed for each configuration using an interest rate of 5%. The costs associated with owning and plant operation depend on the financing type, the capital requirement and the components expected life. The annualized cost method is used to estimate the annual capital cost of system components in this study

for 20 years plant lifetime and plant maintenance factor (ϕ) of 1.06. Table 3 presents the equations used to obtain the annual capital and operating costs using the amortization cost.

c. Exergy-economic model

Levelized annual cost values for all components are used in the evaluation and cost optimization. The hourly capital investment (CI) cost for each component based on the actual annual number of operating hours (N) is calculated as:

$$\dot{Z}^{CI}_{component}(\$/h) = \frac{Z_{component} . CRF . \phi}{N} \tag{13}$$

The exergo-economic analysis is used to estimate the cost rate of the product streams of the system. The cost balance expresses the variable $\dot{C}$ that denotes a cost rate associated with an exergy stream: stream of matter, power, or heat transfer. According to the conservative nature of costs [42], the cost rate associated with the system product $\dot{C}_P \left(\frac{\$}{h}\right)$ is equal to the total rate of expenditure used to generate this product in a component, namely the fuel cost resulting from the cost associated with the exergy flows $\dot{C}_F \left(\frac{\$}{h}\right)$ and the cost rates of the capital investment (CI) and operating and maintenance (OM):

$$\dot{C}_P = \sum \dot{C}_F + \dot{Z}^{CI}_k + \dot{Z}^{O\&M}_k \tag{14}$$

The above cost balance equation is applied to the MED-MVC system components to obtain the product stream cost. Typically, the number of unknown cost parameters is higher than the number of cost balance equations for the component, so additional auxiliary thermodynamic equations are used to accommodate this difference. Usually, the auxiliary equations represent the equality of the average cost of the inlet and exit for the same stream, and they are formulated based on different principles (exergy extraction, multiple outputs, and external assessment) [43]. To include the labor and chemical cost (non-exergy related costs) in the exergo-economic analysis, inlet feed stream to the feed pump was considered

as $\dot{C}_o(\$/h) = (SLC + SCC)(\$/m^3) \times D(m^3/h)$. The total water price ($TWP_{exerg-economic}$) $(\$/m^3)$ from the exergo-economic analysis is calculated by dividing the cost rates of all the outlet streams (distillate and brine) $(\$/h)$ from the MED-MVC unit by the total production rate of the plant (m^3/h).

d. Dynamic model

Following the steady-state solution, a generic dynamic model for a four-effect MED with an MVC unit and two preheaters is developed. Each evaporator effect consists of three lumps: vapor, brine, and tube lump. It is assumed that the accumulation of mass and energy in the evaporator tubes is negligible compared to the accumulation of mass and energy in the brine pool inside an effect [44]. The dynamic model equations of the i^{th} evaporator effect combined lumps mass, energy and salt balances are given by equations (15), (16) and (17), respectively [25]. Each effect is assumed to have a cross-sectional area $A_{ce,i}$ and a total height H_E. The brine pool height $L_{b,i}$ and vapor height $H_E - L_{b,i}$ are shown in Fig. 3 for the ith effect. The brine pool to pool flow between effects is represented by $m_{b,i} = C_{b,i}\sqrt{\Delta P_{b,i}}$ where $\Delta P_{b,i} = P_{i-1} - P_i + \rho_b g\left(L_{b,i-1} - L_{b,i}\right)$ and the vapor flow from one effect to the next is calculated from $m_{v,i} = C_{vi}\sqrt{\Delta P_{vi}}$ where $\Delta P_{vi} = P_{i-1} - P_i$.

$$C_{11}\frac{dL_{b,i}}{dt} + C_{12}\frac{dT_{v,i}}{dt} + C_{13}\frac{\partial X_{b,i}}{\partial t} = C_{14} \quad (15)$$

$$C_{21}\frac{dL_{b,i}}{dt} + C_{22}\frac{dT_{v,i}}{dt} + C_{23}\frac{\partial X_{b,i}}{\partial t} = C_{24} \quad (16)$$

$$C_{31}\frac{dL_{b,i}}{dt} + C_{32}\frac{dT_{v,i}}{dt} + C_{33}\frac{\partial X_{b,i}}{\partial t} = C_{34} \quad (17)$$

where the coefficients ($C_{11}, \ldots\ldots C_{34}$) are shown in Table 4.

The detailed transient characteristics of heat exchangers (HExs) described by partial differential equations are complicated and are not suitable for practical use [45]. Therefore, a lumped model is used to estimate the preheaters outlet temperature variation with time. Both preheaters are considered as counter-flow plate heat exchangers as shown in Fig. 4. The cold stream of seawater feed is heated by

circulating the hot fluid (brine and distillate) through the other side of the plate wall. The last effect brine temperature and distillate mixing temperature represent the hot fluid stream temperatures in the brine and distillate preheaters, respectively. The following assumptions are made in developing the mathematical model for both preheaters [45] where spatial temperature distributions are not considered:

i) Heat losses to the environment are negligible

ii) The heat capacity of fluids is significantly higher than that of the metallic walls.

iii) Mass accumulation inside the pre-heaters is not considered.

Based on the assumptions above, the energy balance equations for the preheaters are presented as:

Brine preheater

$$\frac{\boldsymbol{dT_{F,b}}}{\boldsymbol{dt}} = 2\frac{U_b A_{b,HEx} LMTD_{b,HEx} - \dot{m}_{F,b}\left[T_{F,b}c_{P[T_{F,b},X_f]} - T_{sw}c_{P[T_{sw},X_f]}\right]}{\rho_{[T_{m,F},X_f]}c_{P[T_{m,F},X_f]}\forall_{HEx,channels}} \quad (18)$$

$$\frac{\boldsymbol{dT_{o,b}}}{\boldsymbol{dt}} = 2\frac{\dot{m}_B\left[T_{b,n}c_{P[T_{b,n},X_b]} - T_{o,b}c_{P[T_{o,b},X_b]}\right] - U_b A_{b,HEx} LMTD_{b,HEx}}{\rho_{[T_{m,b},X_b]}c_{P[T_{m,b},X_b]}\forall_{HEx,channels}} \quad (19)$$

Distillate preheater

$$\frac{\boldsymbol{dT_{F,d}}}{\boldsymbol{dt}} = 2\frac{U_d A_{d,HEx} LMTD_{d,HEx} - \dot{m}_{F,d}\left[T_{F,d}c_{P[T_{F,d},X_f]} - T_{sw}c_{P[T_{sw},X_f]}\right]}{\rho_{[T_{m,F},X_f]}c_{P[T_{m,F},X_f]}\forall_{HEx,channels}} \quad (20)$$

$$\frac{\boldsymbol{dT_{o,d}}}{\boldsymbol{dt}} = 2\frac{\dot{m}_D\left[T_{hin,d}c_{P[T_{hind,d}]} - T_{o,d}c_{P[T_{o,b}]}\right] - U_d A_{d,HEx} LMTD_{d,HEx}}{\rho_{[T_{m,d}]}c_{P[T_{m,d}]}\forall_{HEx,channels}} \quad (21)$$

where $\dot{m}$ represents flow rate of the streams of cold and hot fluids (kg/s), c_p is the streams heat capacities (kJ/kg.K), ρ is fluid density (kg/m^3), U is the total heat transfer coefficient (in kW/m^2.K), A is the heat transfer area (m^2) for both preheaters, $\forall$ is the effective volume (m^3) of the preheaters channels, and $LMTD$ is the logarithmic mean temperature difference in the brine and distillate preheaters.

The MVC unit is considered to be in a quasi-steady-state condition since the mechanical vapor compressor has a rapid dynamic response compared to the other heat transfer components. The compressor efficiency η_c is determined by comparing the steady-state isentropic and actual compressor work and is used as an input to the dynamic model. Both the isentropic work and the compressor

isentropic efficiency are used to obtain the instantaneous compression ratio of the MVC unit. From the compression ratio, the inlet steam temperature can be determined. The main differences and commonalities between the present dynamic model for the MED-MVC and the dynamic model for the MED-TVC described in [25] are: (i) the core of the MED which is the evaporator unit is treated the same way using the lumped model developed in [25]; (ii) there is no dynamic model for the condenser unit needed in the MED-MVC, a compressor model is included instead; (iii) two preheater units are dynamically simulated in the MED-MVC; (iv) The MED-TVC system operates on thermal energy from an external source such as a steam power plant or boiler, while the MED-MVC system uses a compressor unit to recycle the vapor from the last effect to the first effect.

As shown in Fig. 5, the steady-state solution procedure for MED-MVC system starts by assuming the brine temperature in all effects and the energy supplied to the first effect. Then, the steady-state conservation equations in Table 1 are solved to obtain the feed and brine flow rates as well as the vapor generated in each effect. The mass flow rate imbalance between the vapor produced in the last effect and the required steam for the first effect is minimized iteratively by modifying the term E_{SH}. This calculation continues until a specified error criterion is achieved (ε=10^{-4}). This value for error criterion is determined to be small enough so that the solution obtained is independent of it. The mixing temperature of the distillate is used to calculate the actual feed temperature by solving the equations of the brine and distillate feed preheaters. The entire calculations are repeated until the specified feed temperature is reached. From the steady-state solution, parameters such as the vapor and brine temperature, the vapor and brine flow rate and salinity at each effect are used as initial input for the dynamic model calculations. A FORTRAN code is developed to solve both the steady-state and dynamic models. The system of ordinary differential equations is solved by using the fourth-order Runge-Kutta method. By solving Eqs. (15)-(21), the vapor temperature, brine level, effect salinity, preheaters outlet temperatures and supplied feed temperature are obtained at each time step. The brine and vapor flow rates between effects are adjusted based on the vapor

pressure calculated in the effects. In the dynamic model, the compressor work and seawater temperature can be disturbed with different intensities from the steady-state condition for a pre-specified duration. Indicator parameters such as the effect temperature, brine level and vapor flow across effects are calculated with time. The performance indicator parameters such as PR and SPC are obtained as well.

Results and discussion

a. Steady-state operation and exergo-economic analysis

The focus of this study is to present a generic steady-state and dynamic model which can be easily modified to describe any number of effects for MED-MVC systems and two independent preheaters for the inlet seawater. The steady-state model is validated using the actual operational parameters of MED-MVC plant located in Flamanville, France [32], which operates with four effects in s parallel/cross feed configuration integrated with a MVC unit. Table 5 shows the currently steady-state model resulting values for the process variables which show excellent agreement compared with the data reported in [32]. Exergy analysis overcomes the shortcomings of energy analysis by identifying the causes, locations and actual magnitudes of waste due to thermodynamic inefficiencies [10]. The minimum work of separation $\dot{W}_{min}$ for the separation of 39.44 kg/s of seawater into 17.6 kg/s of fresh water and 21.84 kg/s of brine with a salinity of 65 ppt at the same temperature and pressure can be determined independently by using the relation developed by Cerci [46]. For a recovery ratio of ~40%, the relation gives 28.16 kW, which is sufficiently close to the result obtained from equation (12).

There are two causes of exergy destruction in the MED systems. The first is due to the heat transfer across the temperature difference between hot and cold streams in each evaporator effect and the preheaters. Also, exergy destructions in the pump and compressor are due to irreversibilities in the pump and compression processes. The exergy destruction (kW) for the main components of MED-MVC are presented in Fig. 6. A significant source of exergy destruction occurs in MVC unit (39%) and evaporators (52.6%). This can be attributed to the thermodynamic inefficiency of the MVC unit and the heat transfer

in the effects that are associated with phase change processes. The high exergy destructions in the evaporators indicate that the evaporation process itself is highly inefficient. Therefore, modifications and improvements to the process must be considered. This can be reduced by increasing the number of effects, though the number is limited by the operating compression ratio of MVC units currently available. Also, the economic consideration due to increasing the heat transfer surface needed to achieve evaporation and condensation processes should be accounted. Other components such as brine and distillate feed heaters introduce exergy destructions that nearly equal to 7.0%. Moreover, Fig. 6 indicates that the highest exergetic efficiencies belong to pumps. It should be noted that the exergetic efficiency of the MED-MVC plant is quite low (2.82%), which reveals its high irreversibilities that is close to the values presented in the reported literature [12, 47].

A simple conventional economic model treating the MED-MVC plant as a whole unit is used to calculate the annualized cost of the plant and to estimate the total water price for a MED-MVC system. The total levelized fixed cost associated with CI&IM of the components per hour basis is 19.98 $/h. The most expensive components are the evaporators (~10.13 $/h) while the cheapest are the pumps (~0.3 $/h). The costs for the MVC unit and the preheaters are 7.3 and 1.3 $/h, respectively. However, to indicate the contribution of each flow stream and each component in the final product cost, an exergo-economic analysis is applied to all MED-MVC components and flow streams. When conducting a thermoeconomic analysis for the current MED-MVC system, a cost balance equation is used to correlate the exergy instead of the energy of the flow stream with the pricing value of the component. The exergy-cost unit analysis is more reasonably distributed and is meaningful than the energy-based ones. The non-exergy related costs represented by chemical cost and labor cost are added to the exergo-economic model as input stream in the feed seawater. Further, it should be mentioned that there is no additional information to appropriately apportion the value of other cost and indirect cost between the product streams (distillate and brine) in the cost exergy equations. The other costs (80K $) and indirect capital costs (0.15 DCC)

are calculated on a per hour basis, and a value of 3.65 $/h is obtained. For simplicity, these costs are divided equally between distillate and brine streams. Solving the exergy-cost balance equations, the cost rates for various streams at different locations in the MED-MVC plant are obtained. The cost rate pricing for all flow streams through the MED-MVC system of 1500 m^3/day production capacity is shown as a diagram in Fig. 6 with the estimated production cost of 1.70 and 1.63 $/$m^3$ using simple conventional economic model and exergy-based cost model, respectively. Both methods results are consistent with the results for MED-MVC desalination system and similar systems found in the literature [12, 40, 48]. Besides showing the cost flow rate at each stream point, the figure shows flow exergy, temperature and stream flow rate as well. To some extent, both methods (simple economical method and the exergo-economic method) have a similar estimation for the final product price (freshwater). However, the exergo-economic method slightly underestimates the water price, and this is directly attributed to the assumptions used in the auxiliary equations and the uncertainty associated with the cost due to round-off [43].

The primary contributor to the SPC in a MED-MVC system is the power required for the MVC unit which depends on the compressor efficiency, compression ratio and inlet vapor specific volume. The operation cost can be reduced by increasing the performance ratio (PR) or decreasing the SPC. Therefore, efforts are made to reduce the cost associated with the MVC. This can be done by reducing the vapor flow rate through the MVC unit by installing more effects N while keeping the same overall temperature difference. On the other hand, capital cost can be reduced by reducing the required specific heat transfer area (S_A) for the evaporators and pre-heaters units. For the MED-MVC, to decrease the S_A, the TBT must be increased. The increase in TBT may require specific chemical pre-treatments and add cost for better tube material and higher maintenance. Increasing N has its limits as this increases the required S_A for evaporation due to the decrease in the temperature difference between the effects. Consequently, capital cost savings should be considered along with the increase in operating cost. It is essential to determine

the optimal balance between the design parameters of N and TBT that achieves the best economic operation. The decrease in the SPC with increasing the number of effects N has its limit as shown in Fig. 7. A single-effect MVC has the highest SPC due to the amount of vapor flow (displacement volume) through the MVC unit, leading to the highest TWP. Adding a second effect increases the η_{II} and reduces the SPC as shown in Fig. 7. Although this increases the S_A, the TWP reduces to ~ 1.6 \$/m^3 due to a reduction in the operating cost of the MVC unit. Further increase in the number of effects from 2 to 6 brings little increase in the η_{II} and little change in the SPC. On the other hand, the TWP keeps increasing with the increase in N which is due to the continuous increase in S_A (capital cost). Increasing N beyond 6 leads to an increase in the SPC and a decrease in η_{II} for a fixed production capacity. This is attributed to the large decrease in the volumetric vapor flow rate through the MVC unit which may not be sufficient to generate the required amount of vapor in the first effect. Increasing the number of effects from 2 to 10 causes an increase in the TWP by 16% approximately. The main reason for not using multiple effects beyond 6 in MVC systems is the practical limitation of the displacement volume of the commercially available compressors [49].

b. Dynamic analysis

First, the dynamic model results are justified with a three-effects lab-scale MED plant with a total production capacity of 3 m^3/day. The detailed description of the steady-state operating conditions of the 3-effect plant and the results of the dynamic model validation are presented in [25]. In a real application, the operational conditions may not be kept constant due to the changes in climate conditions and the rate of the designed heat source flow rate or electrical power to the plant. These fluctuations from the design steady-state values may i) cause the plant to approach a new steady-state condition; ii) agitate the plant performance thus causing production capacity changes; or iii) in some occasions, lead the plant to reach dry out or flooding. Thus, the model describes the relationships between the disturbance input parameters (compressor work and inlet seawater temperature) and the output process variables (effects temperature,

brine level, brine flowrate and vapor flow rate). A linear change in the main input parameters is considered that form a ramped type disturbance with the pre-specified magnitude of change and applied duration. Based on the actual evaporator configuration dimensions, the initialized brine level was chosen as 0.25 m [50]. Two limitations are assigned on the brine level, $L_b < 1.0$ m and $L_b > 0.1$ m to avoid flooding or dry out conditions, respectively.

In some situations, a disturbance (or fluctuation) is applied to the work supplied to the MVC unit to change total plant output. If intentional, this change is called “turndown“ and is carried out to address the power demand swings [16]. This turndown ratio may reach 50%, meaning the minimum flow is half of the maximum design flow. The system variables namely: brine level, vapor temperature, supplied steam temperature, brine flow rate and vapor flow rate are calculated to assess the impact of a 10% ramp reduction in the supplied compressor work on the system variables as shown in Fig. 8. The applied ramp reduction starts at the time of 5,000 s with a ramp time of 1,000 s. The system is allowed to run with this reduced compressor work until it reaches another steady-state condition. The reduction in the supplied energy to the MVC unit causes a decrease in the compression ratio and the temperature of the supplied steam to the first effect. The response of the vapor lump in each effect is much faster than the response of the liquid lump (brine level) due to the higher thermal capacity of the liquid compared to that of the vapor. Consequently, a reduction in the vapor temperature and pressure in all effects is experienced at the beginning of the disturbance. This leads to a gradual decrease in the brine and condensed vapor flow rates in the preheaters, which in turn decreases the feed temperature to the effects. Furthermore, the steam temperature decreases due to the reduction in the vapor temperature in the last effect. The reduction in both vapor and feed temperatures eventually results in more accumulation of the brine in the effects and increases the brine level as shown in Fig. 8. The build-up in the brine level causes the hydrostatic pressure for the brine lump to increase, pushing the hot brine to flow from one effect to the next and to cause the

feed temperature to rise. This increase in the feed temperature enhances the vapor temperature and slightly reduces the brine level to attain a new steady-state operating condition.

Figure 9 shows the effect of the application of a 10% increase in the inlet seawater temperature (2.5^{o}C) on the plant process variables. At the beginning of the disturbance, the feed temperature to all effects increases at the same time. This improves the evaporation rate and increases the vapor temperature in all the effects and the increase in vapor pressure inside the effects increases the brine flow rate. However, the reduction in the brine level causes a gradual decrease in the brine flow rate as shown in Fig. 9. The dynamic response of the feed preheaters to the variations in brine and distillate flow rates causes the vapor temperature and vapor flow rate to go up before they reach their steady-state values as shown in Fig. 9.

The economics, steady-state performance and transient behavior of a MED–MVC system are compared to those of a MED-TVC system with a similar production capacity. The MED-TVC system, operating with four effects and a bottom condenser, is investigated using the model developed by Elsayed et al. [25] under the same constraints for the freshwater production rate (17.6 kg/s) and rejected brine salinity (65 ppt). The calculated values of the GOR and TWP for a fresh water production rate of 1500 m^3/d are 3.99 and 1.6 \$/m^3, respectively for the MED–MVC, and 6.4 and 2.6 \$/m^3, respectively for the MED-TVC. Dynamic simulations for both systems under a 15% reduction in the inlet seawater temperature (3.75^{o}C) are performed. As shown in Fig. 10, the MED-TVC is rather sensitive to the decrease in seawater temperature which affects the condenser unit as mentioned in Elsayed et al. [25]. This sensitivity causes a significant increase and decrease in the brine level and production capacity, respectively in the MED-TVC system compared to the MED-MVC system. The MED-MVC system has a slower response due to the high thermal capacity of the brine/distillate feed preheaters compared to the low thermal capacity of the condenser's vapor lump in the MED-TVC system.

Next, the effect of the intensity of the applied disturbances on the vapor temperature and brine level of the first effect is shown in Fig. 11. The compressor work and seawater temperature have been reduced by up to 30% and 25% of the steady-state values, respectively. For the current MED-MVC configuration and dimensions, it is noted that a significant reduction in compressor work could lead to a substantial decrease in the temperature difference between the first effect brine and the steam at compressor exit. For instance, the steam temperature supplied by the MVC unit approaches the brine pool temperature for a 30% reduction in the compressor work. In this case, although the evaporation can still occur between the sprayed feed and the steam temperature inside the tubes, the hot brine pool temperature will drop with time, and the brine level in the 1st effect will reach the flooding condition. In addition to approaching the flooding condition, operating the MED-MVC evaporator unit at higher brine levels than designed may lead to salt deposition and light scaling at the bottom of the tubes [51]. The reduction in the inlet seawater temperature reduces the feed temperature causing the brine level to increase, but it does not affect the temperature difference between the steam supplied and the first effect temperature brine. However, as shown in Fig. 9, increasing the seawater temperature above 10% of the steady-state condition would lead to dry out in the first effect evaporator. A dry out condition means the vapor generated in the 1st effect may storm through the 2nd effect. This blowout of the vapor through the brine pipes will perturb the brine flashing and feed evaporation processes where the plant may be exposed to operational failure.

A plot of the variations of the PR, SPC and total distillate production with step changes in the compressor work and inlet seawater temperature is shown in Fig. 12. The dependence of PR and SPC on $\dot{W}_c$ and T_{sw} is approximately linear. As shown in Fig. 12a, a decrease in the compressor work below the steady-state designed condition decreases the condensation rate (distillate) in each effect. But since the magnitude of the decrease in the total distillate production rate is less than the reduction in compressor work, PR increases and SPC decreases. A reduction in inlet seawater temperature results in a decrease in

the production of fresh water, brine blowdown temperature and PR which in turn causes an increase in SPC for the same supplied compressor work [34]. The reduction in the supplied seawater temperature decreases the TBT which leads to a decrease in the brine flashing and seawater evaporation rates in all effects as shown in Fig. 12b. This results in less vapor generation and higher brine level increase in all the effects.

Conclusions

Within the current work, a new formulation for the steady-state thermodynamic model of MED-MVC desalination systems operating in parallel/cross configuration has been presented. The steady-state solution reveals that the η_{II} is 2.82%. The exergy destructions in the MVC unit and evaporators combine to approximately 90% of the total exergy destruction in the system. The most expensive components are the evaporator units with a cost of ~10.13 $/h compared to 7.3, 1.3 and 0.3 $/h for MVC unit, preheaters and pumps, respectively. The TWP for the MED-MVC with a 1500 m^3/day production capacity is 1.70 and 1.63 $/$m^3$ using a simple conventional economic model and a specific exergy cost model, respectively. Sensitivity analysis shows that a two-effect MVC system is superior to the single-effect MVC system, but the number of effects N that can be implemented is limited. Increasing N from 2 to 6 results in little change in the SPC or η_{II} . On the other hand, the value of TWP increases by approximately 16% as N increases from 2 to 10.

The dynamic model results show that the disturbances in compressor work have a significant effect on the plant transient behavior while a disturbance in the inlet seawater temperature has only a moderate impact. A reduction in compressor work leads to a reduction in the steam temperature that causes an increase in the effects brine level. For instance, the steam temperature supplied by the MVC unit approaches the brine pool temperature when a 30% reduction in the compressor work occurs. So, any further decrease in compressor work may lead to flooding in the effects and the plant may cease to operate. A decrease in the inlet seawater temperature reduces the feed temperature causing the brine level

to increase, but this does not affect the temperature difference between the steam supplied and the first effect temperature. On the other hand, increasing the seawater temperature above 10% of the steady-state condition without proper control on the plant response could lead to dry out in the effects. Thermo-economic and dynamic response comparisons between the MED-MVC and MED-TVC systems reveal that: (i) the TWP for the MED-TVC is higher than the MED-MVC; (ii) the MED-TVC is more sensitive to the reduction in the seawater temperature than the MED-MVC; (iii) the MED-MVC is slower in response compared to the MED-TVC. In term of performance, a reduction in compressor work causes a decrease in the plant total distillate production capacity, but an increase in PR and a decrease in SPC. On the other hand, a reduction in the inlet seawater temperature decreases the TBT, which causes a decrease in brine flashing and feed evaporation rates with an increase in the brine levels in the effects. This leads to a reduction in the production of fresh water, a decrease in PR and an increase in the SPC for the same supplied compressor work.

Acknowledgments

This work is supported by Department of Energy (DOE) through the Grant No. DE-SC0015809 and the Egyptian Ministry of Research and Higher Education.

References

[1] K. Thu, Y.-D. Kim, A. Myat, A. Chakraborty, K.C. Ng, Performance investigation of advanced adsorption desalination cycle with condenser–evaporator heat recovery scheme, Desalination and Water Treatment, 51 (2013) 150-163. https://doi.org/10.1080/19443994.2012.693659.

[2] M.W. Shahzad, K.C. Ng, K. Thu, B.B. Saha, W.G. Chun, Multi effect desalination and adsorption desalination (MEDAD): A hybrid desalination method, Applied Thermal Engineering, 72 (2014) 289-297. https://doi.org/10.1016/j.applthermaleng.2014.03.064.

[3] H. Lu, J. Wang, T. Wang, N. Wang, Y. Bao, H. Hao, Crystallization techniques in wastewater treatment: An overview of applications, Chemosphere, 173 (2017) 474-484. https://doi.org/10.1016/j.chemosphere.2017.01.070.

[4] L. Weimer, T. Fosberg, L. Musil, Maximizing water recovery/reuse via mechanical vapor-recompression (MVR) evaporation, Environmental Progress & Sustainable Energy, 2 (1983) 246-250. https://doi.org/10.1002/ep.670020410.

[5] M. Sharaf, A. Nafey, L. García-Rodríguez, Thermo-economic analysis of solar thermal power cycles assisted MED-VC (multi effect distillation-vapor compression) desalination processes, Energy, 36 (2011) 2753-2764. https://doi.org/10.1016/j.energy.2011.02.015.

[6] A. Helal, S. Al-Malek, Design of a solar-assisted mechanical vapor compression (MVC) desalination unit for remote areas in the UAE, Desalination, 197 (2006) 273-300. https://doi.org/10.1016/j.desal.2006.01.021.

[7] C.R. Henderson, J.F. Manwell, J.G. McGowan, A wind/diesel hybrid system with desalination for Star Island, NH: feasibility study results, Desalination, 237 (2009) 318-329. https://doi.org/10.1016/j.desal.2005.07.054.

[8] D. Zejli, A. Ouammi, R. Sacile, H. Dagdougui, A. Elmidaoui, An optimization model for a mechanical vapor compression desalination plant driven by a wind/PV hybrid system, Applied energy, 88 (2011) 4042-4054. https://doi.org/10.1016/j.apenergy.2011.04.031.

[9] M.H. Sharqawy, S.M. Zubair, On exergy calculations of seawater with applications in desalination systems, International Journal of Thermal Sciences, 50 (2011) 187-196. https://doi.org/10.1016/j.ijthermalsci.2010.09.013.

[10] N. Kahraman, Y.A. Cengel, Exergy analysis of a MSF distillation plant, Energy Conversion and Management, 46 (2005) 2625-2636. https://doi.org/10.1016/j.enconman.2004.11.009.

[11] F.N. Alasfour, H.K. Abdulrahim, The effect of stage temperature drop on MVC thermal performance, Desalination, 265 (2011) 213-221. https://doi.org/10.1016/j.desal.2010.07.054.

[12] A. Nafey, H. Fath, A. Mabrouk, Thermoeconomic design of a multi-effect evaporation mechanical vapor compression (MEE–MVC) desalination process, Desalination, 230 (2008) 1-15. https://doi.org/10.1016/j.desal.2007.08.021.

[13] M. Ahmadi, E. Baniasadi, H. Ahmadikia, Process modeling and performance analysis of a productive water recovery system, Applied Thermal Engineering, 112 (2017) 100-110. https://doi.org/10.1016/j.applthermaleng.2016.10.067.

[14] T. Tong, M. Elimelech, The global rise of zero liquid discharge for wastewater management: drivers, technologies, and future directions, Environmental science & technology, 50 (2016) 6846-6855. https://doi.org/10.1021/acs.est.6b01000.

[15] A. Husain, A. Hassan, D.M. Al-Gobaisi, A. Al-Radif, A. Woldai, C. Sommariva, Modelling, simulation, optimization and control of multistage flashing (MSF) desalination plants Part I: Modelling and simulation, Desalination, 92 (1993) 21-41. https://doi.org/10.1016/0011-9164(93)80074-W.

[16] D. Dietrich, Enhanced Digital Control of a Mechanical Recompression Evaporator in a Modern Fructose Refinery, Starch - Stärke, 37 (1985) 149-154. https://doi.org/10.1002/star.19850370502.

[17] M. Mazzotti, M. Rosso, A. Beltramini, M. Morbidelli, Dynamic modeling of multistage flash desalination plants, Desalination, 127 (2000) 207-218. https://doi.org/10.1016/S0011-9164(00)00011-4.

[18] L. Roca, L.J. Yebra, M. Berenguel, D.C. Alarcón-Padilla, Modeling of a solar seawater desalination plant for automatic operation purposes, Journal of Solar Energy Engineering, 130 (2008) 041009. https://doi.org/10.1115/1.2969807.

[19] A. de la Calle, J. Bonilla, L. Roca, P. Palenzuela, Dynamic modeling and performance of the first cell of a multi-effect distillation plant, Applied Thermal Engineering, 70 (2014) 410-420. https://doi.org/10.1016/j.applthermaleng.2014.05.035.

[20] A. de la Calle, J. Bonilla, L. Roca, P. Palenzuela, Dynamic modeling and simulation of a solar-assisted multi-effect distillation plant, Desalination, 357 (2015) 65-76. https://doi.org/10.1016/j.desal.2014.11.008.

[21] L. Roca, J.A. Sánchez, F. Rodríguez, J. Bonilla, A. de la Calle, M. Berenguel, Predictive control applied to a solar desalination plant connected to a greenhouse with daily variation of irrigation water demand, Energies, 9 (2016) 194.

[22] N.H. Aly, M. Marwan, Dynamic response of multi-effect evaporators, Desalination, 114 (1997) 189-196. https://doi.org/10.1016/S0011-9164(98)00011-3.

[23] M.T. Mazini, A. Yazdizadeh, M.H. Ramezani, Dynamic modeling of multi-effect desalination with thermal vapor compressor plant, Desalination, 353 (2014) 98-108. https://doi.org/10.1016/j.desal.2014.09.014.

[24] A. Cipollina, M. Agnello, A. Piacentino, A. Tamburini, B. Ortega, P. Palenzuela, D. Alarcon, G. Micale, A dynamic model for MED-TVC transient operation, Desalination, 413 (2017) 234-257. https://doi.org/10.1016/j.desal.2017.03.005.

[25] M.L. Elsayed, O. Mesalhy, R.H. Mohammed, L.C. Chow, Transient performance of MED processes with different feed configurations, Desalination, 438 (2018) 37-53. https://doi.org/10.1016/j.desal.2018.03.016.

[26] K. El-Khatib, A.A. El-Hamid, A. Eissa, M. Khedr, Transient model, simulation and control of a single-effect mechanical vapour compression (SEMVC) desalination system, Desalination, 166 (2004) 157-165. https://doi.org/10.1016/j.desal.2004.06.070.

[27] G. Kishore, S. Nisan, S. Dardou, A. Adak, V. Srivastava, P. Tewari, Development of a dynamic simulator (INFMED) for the MED/VC plant, Desalination and Water Treatment, 21 (2010) 364-374. https://doi.org/10.5004/dwt.2010.1752.

[28] J. Winchester, C. Marsh, Dynamics and control of falling film evaporators with mechanical vapour recompression, Chemical Engineering Research and Design, 77 (1999) 357-371. https://doi.org/10.1205/026387699526340.

[29] H. Ettouney, Design of single-effect mechanical vapor compression, Desalination, 190 (2006) 1-15. https://doi.org/10.1016/j.desal.2005.08.003.

[30] V.C. Onishi, A. Carrero-Parreño, J.A. Reyes-Labarta, R. Ruiz-Femenia, R. Salcedo-Díaz, E.S. Fraga, J.A. Caballero, Shale gas flowback water desalination: Single vs multiple-effect evaporation with vapor recompression cycle and thermal integration, Desalination, 404 (2017) 230-248. https://doi.org/10.1016/j.desal.2016.11.003.

[31] R. Matz, Z. Zimerman, Low-temperature vapour compression and multi-effect distillation of seawater. Effects of design on operation and economics, Desalination, 52 (1985) 201-216. https://doi.org/10.1016/0011-9164(85)85009-8.

[32] M. Lucas, B. Tabourier, The mechanical vapour compression process applied to seawater desalination: a 1,500 ton/day unit installed in the nuclear power plant of Flamanville, France, Desalination, 52 (1985) 123-133. https://doi.org/10.1016/0011-9164(85)85003-7.

[33] N.H. Aly, A.K. El-Figi, Mechanical vapor compression desalination systems—a case study, Desalination, 158 (2003) 143-150. https://doi.org/10.1016/S0011-9164(03)00444-2.

[34] H.T. El-Dessouky, H.M. Ettouney, Fundamentals of salt water desalination, Elsevier, 2002.

[35] J. Veza, Mechanical vapour compression desalination plants—A case study, Desalination, 101 (1995) 1-10. https://doi.org/10.1016/0011-9164(95)00002-J.

[36] M.W. Shahzad, M. Burhan, H.S. Son, S.J. Oh, K.C. Ng, Desalination processes evaluation at common platform: A universal performance ratio (UPR) method, Applied Thermal Engineering, 134 (2018) 62-67. https://doi.org/10.1016/j.applthermaleng.2018.01.098.

[37] Z.H. Ayub, Plate heat exchanger literature survey and new heat transfer and pressure drop correlations for refrigerant evaporators, Heat transfer engineering, 24 (2003) 3-16. https://doi.org/10.1080/01457630304056.

[38] J.A. Carballo, J. Bonilla, L. Roca, A. De la Calle, P. Palenzuela, D.C. Alarcón-Padilla, Optimal operating conditions analysis for a multi-effect distillation plant according to energetic and exergetic criteria, Desalination, 435 (2018) 70-76. https://doi.org/10.1016/j.desal.2017.12.013.

[39] M.M. El-Halwagi, Sustainable design through process integration: fundamentals and applications to industrial pollution prevention, resource conservation, and profitability enhancement, Butterworth-Heinemann, 2017.

[40] N. Lukic, L. Diezel, A. Fröba, A. Leipertz, Economical aspects of the improvement of a mechanical vapour compression desalination plant by dropwise condensation, Desalination, 264 (2010) 173-178. https://doi.org/10.1016/j.desal.2010.07.023.

[41] H. Ozcan, I. Dincer, Exergoeconomic optimization of a new four-step magnesium–chlorine cycle, International Journal of Hydrogen Energy, 42 (2017) 2435-2445. https://doi.org/10.1016/j.ijhydene.2016.03.098.

[42] S. Usón, A. Valero, A. Agudelo, Thermoeconomics and industrial symbiosis. Effect of by-product integration in cost assessment, Energy, 45 (2012) 43-51. https://doi.org/10.1016/j.energy.2012.04.016.

[43] A. Bejan, G. Tsatsaronis, Thermal design and optimization, John Wiley & Sons, 1996.

[44] J. Burdett, C. Hollanu, Dynamics of a multiple-effect evaporator system, AIChE Journal, 17 (1971) 1080-1089. https://doi.org/10.1002/aic.690170512.

[45] N. Abbasov, R. Zeinalov, O. Azizova, S. Imranova, Dynamic models of heat exchangers, Chemistry and technology of fuels and oils, 42 (2006) 25-29. http://dx.doi.org/10.1007/s10553-006-0022-2.

[46] Y. Cerci, The minimum work requirement for distillation processes, Exergy, An International Journal, 2 (2002) 15-23. https://doi.org/10.1016/S1164-0235(01)00036-X.

[47] F. Hafdhi, T. Khir, A.B. Yahia, A.B. Brahim, Exergoeconomic optimization of a double effect desalination unit used in an industrial steam power plant, Desalination, 438 (2018) 63-82. https://doi.org/10.1016/j.desal.2018.03.020.

[48] S. Frioui, R. Oumeddour, Investment and production costs of desalination plants by semi-empirical method, Desalination, 223 (2008) 457-463. https://doi.org/10.1016/j.desal.2007.01.180.

[49] M. Darwish, Thermal analysis of vapor compression desalination system, Desalination, 69 (1988) 275-295. https://doi.org/10.1016/0011-9164(88)80030-4.

[50] O. Kotb, Optimum numerical approach of a MSF desalination plant to be supplied by a new specific 650 MW power plant located on the Red Sea in Egypt, Ain Shams Engineering Journal, 6 (2015) 257-265. https://doi.org/10.1016/j.asej.2014.09.001.

[51] P. Budhiraja, A.A. Fares, Studies of scale formation and optimization of antiscalant dosing in multi-effect thermal desalination units, Desalination, 220 (2008) 313-325. https://doi.org/10.1016/j.desal.2007.01.036.

[52] W. El-Mudir, M. El-Bousiffi, S. Al-Hengari, Performance evaluation of a small size TVC desalination plant, Desalination, 165 (2004) 269-279. https://doi.org/10.1016/j.desal.2004.06.031.

[53] Y. El-Sayed, Designing desalination systems for higher productivity, Desalination, 134 (2001) 129-158. https://doi.org/10.1016/S0011-9164(01)00122-9.

Nomenclature

Latin

A	Heat transfer area m^2
A_{ce}	Cross section area of evaporator, m^2
A_{cc}	Cross section area of condenser, m^2
BPE	Boiling point elevation °C
C_b	Discharge coefficient for brine flow
C_v	Discharge coefficient for vapor flow
C_p	Specific heat capacity at constant pressure, kJ/kg °C
C_r	Compression ratio
D	Total distillate flow rate, kg/s
$\dot{E}$	Exergy, kW
GOR	Gain output ratio
h	Enthalpy of saturated water, kJ/kg
H	Total height, m
L	Level, m
m_{vg}	Vapor generated kg/s
M	Lump mass kg
m	Mass flow rate kg/s
P	Pressure, kPa
ppt	Part per thousand, g/kg
Q	Heat transfer rate, kW
t	Time, hr
T_{feed}	Seawater feed temperature, ^oC
$T_{hin,d}$	Distillate mix temperature, ^oC
TBT	Top brine temperature, ^oC
U	Overall heat transfer coefficient, $kW/m^2.K$
$\dot{W}$	Work, kW

Greek

ρ	density, kg m^{-3}
∀	Volume, m^3
λ	Latent heat of vaporization, kJ/kg
ε	Error criteria
δ	Difference

Subscripts:

b	brine
d	distillate
f	feed
L	liquid
v	vapor
t	Tube
s	steam
sat	Saturation
i	Effect number
n	Last effect
o	out
sw	seawater
E	Evaporator/effect
SH	superheat

Abbreviation

MED	Multi-effect desalination
MVC	Mechanical vapor compression
PR	Performance ratio
SPC	Specific power consumption
TVC	Thermal vapor compressor

Table captions

Table 1. Conservation equations for a MED-MVC system.

Table 2. Purchased cost equations for MED-MVC system components.

Table 3. Simple cost model equation for MED-MVC system.

Table 4. Rate coefficients of the i[th] effect dynamic equations for a MED-MVC system.

Table 5. Operational steady-state conditions for MED-MVC system.

Table 1 Conservation equations for a MED-MVC system.

Equations	First effect	Second to last effect (n)	F	B	D
Mass	$B_1 = F_1 - D_1$	$B_i = F_i - D_i + B_{i-1} - d_i$	$\sum_{i=1}^{n} F_i$	B_n	$\sum_{i=1}^{n} D_i + d_i$
Salt	$F_1.X_f = B_1.X_1$	$B_i.X_i = B_{i-1}.X_{i-1} + F_i.X_f$			
Energy	$D_1 = \frac{Q_{s,1} - F_1(h_1 - h_f)}{\lambda_1}$, $d_1 = 0$	$D_i = \frac{(D_{i-1} + d_{i-1}).\lambda_{i-1}}{\lambda_i} - \frac{F_i(h_i - h_f)}{\lambda_i}$, $d_i = \frac{B_{i-1}(h_{i-1} - h_i)}{\lambda_i}$			
Total mass balance $F = B + D$					
Total salt balance $F.X_f = B.X_n$					
d_i , Vapor produced by brine flashing.					
D, Total distillate flow rate.					
F, Total feed flow rate.					
B, Total brine flow rate.					

Table 2 Purchased cost equations for MED-MVC system components.

Component	Purchase cost (Z_k) ($)	Comments	Ref.
Preheater (heat exchanger)	$\mathbf{Z_{preheater} = 1000(12.82 + A_{Hex}^{0.8})}$	S for shell side and t for tube side, dp (kPa), A (m^2), U $(kW/m^2.k)$	[52]
MED effect (evaporator)	$\mathbf{Z_{effect} = 250.26 \times UA_{evaporator} dp_t^{-0.01} dp_s^{-0.1}}$		[53]
Water pump	$\mathbf{Z_{pump} = 13.92 \times \dot{m}_{water}^{0.55} \Delta P^{0.55} \left(\frac{\eta_p}{1-\eta_p}\right)^{1.05}}$	$\eta_p = 0.9$, ΔP (kPa)	
Compressor (MVC)	$\mathbf{Z_{MVC} = 794.68 \times \dot{W}_{compressor} + 66.11}$	$\dot{W}_{compressor}$ (Watt)	[40]
Other direct costs	$\mathbf{Z_{rest} = 21635.4 \times D^{0.1773}}$	D (m^3/day)	

Table 3 Simple cost model equation for MED-MVC system.

Parameter	Equation	Comments	Ref.
Capital recovery factor, 1/y	$\boldsymbol{CRF = \frac{i.(1+i)^{nt}}{(1+i)^{nt}-1}}$	i is the interest rate 5%, nt (20 year)	[34]
Annual fixed costs, $/y	$\boldsymbol{AFC = (1.38 \times DCC) \times CRF}$		
Annual electric power cost, $/y	$\boldsymbol{AEPC = C_e.SPC.D/\phi}$	Specific electricity cost $\boldsymbol{C_e = 0.08 \frac{\$}{kWh}}$	
Annual chemical cost, $/y	$\boldsymbol{ACC = SCC.D/\phi}$	Specific chemical cost $\boldsymbol{SCC = 0.025 \frac{\$}{m^3}}$	
Annual labor cost, $/y	$\boldsymbol{ALC = SLC.D/\phi}$	Specific labor cost $\boldsymbol{SLC = 0.1 \frac{\$}{m^3}}$	
Operating and maintenance annual costs, $	$\boldsymbol{OMC = 0.02 \times CRF \times DCC}$		
Total annual cost, $/y	$\boldsymbol{TAC = AFC + AEPC + ACC + ALC + OMC}$		
Total water price $/$m^3$	$\boldsymbol{TWP_{simple} = \frac{TAC.\phi}{D}}$	D $(\frac{m^3}{year})$	

Table 4 Rate coefficients of the i[th] effect dynamic equations for a MED-MVC system.

C_{11}	C_{12}	C_{13}	C_{14}
$A_{ce,i}(\rho_{b,i} - \rho_{v,i})$	$\left[A_{ce,i}L_{b,i}\frac{d\rho_{b,i}}{dT_{b,i}}\left(1+\frac{\partial BPE}{\partial T_{v,i}}\right)+(H_E-L_{b,i})A_{ce,i}\frac{d\rho_{v,i}}{dT_{v,i}}\right]$	$\left[A_{ce,i}L_{b,i}\left\{\frac{d\rho_{b,i}}{dT_{b,i}}\frac{\partial BPE}{\partial X_{b,i}}+\frac{d\rho_{b,i}}{dX}\right\}\right]$	$m_{f,i}+m_{b,i-1}-m_{b,i}-m_{v,i}$
C_{21}	C_{22}	C_{23}	C_{24}
$A_{ce,i}(\rho_{b,i}h_{b,i} - \rho_{v,i}h_{vi})$	$\left[A_{ce,i}L_{b,i}\left\{\rho_{b,i}\frac{dh_{b,i}}{dT_{b,i}}+h_{b,i}\frac{d\rho_{b,i}}{dT_{b,i}}\right\}\left(1+\frac{\partial BPE}{\partial T_{v,i}}\right)+(H_E-L_{b,i})A_{ce,i}\left\{\rho_{v,i}\frac{dh_{v,i}}{dT_{v,i}}+h_{v,i}\frac{d\rho_{v,i}}{dT_{v,i}}\right\}\right]$	$\left[A_{ce,i}L_{b,i}h_{b,i}\left(\frac{d\rho_{b,i}}{dT_{b,i}}\frac{\partial BPE}{\partial X_{b,i}}+\frac{d\rho_{b,i}}{dX}\right)+A_{ce,i}L_{b,i}\rho_{b,i}\frac{dh_{b,i}}{dT_{b,i}}\frac{\partial BPE}{\partial X_{b,i}}\right]$	$m_{f,i}h_{f,i}+m_{b,i-1}h_{b,i-1}-m_{b,i}h_{b,i}+Q_{s,1}$
C_{31}	C_{32}	C_{33}	C_{34}
$A_{ce,i}\rho_{b,i}X_{b,i}$	$\left[A_{ce,i}L_{b,i}X_{b,i}\frac{d\rho_{b,i}}{dT_{b,i}}\left(1+\frac{\partial BPE}{\partial T_{v,i}}\right)\right]$	$\left[A_{ce,i}L_{b,i}\left\{X_{b,i}\frac{d\rho_{b,i}}{dT_{b,i}}\frac{\partial BPE}{\partial X_{b,i}}+\rho_{b,i}+X_{b,i}\frac{d\rho_{b,i}}{dX}\right\}\right]$	$m_{f,i}X_{f,i}+m_{b,i-1}X_{b,i-1}-m_{b,i}X_{b,i}$

Table 5 Operational steady-state conditions for MED-MVC system.

Configuration	**Model**	Flamanville [32]	**% error**
Inlet seawater temperature, °C		25	--
Feed content in, g/kg		36	--
Brine content out, g/kg		65	--
Steam temperature T_s, °C		62.5	--
last effect brine temperature T_n, °C		50.3	--
Pressure ratio	1.85	1.86	0.5
Distillate production (D), m^3/h	64.0	62.5	2.4
Feed flow (F), m^3/h	141.45	140	1
Brine flow (B), m^3/h	78.34	77.5	1
Feed temperature T_f, °C	48.03	49	1.9
Compressor actual work ($\dot{W}_{comp}$), kW	690	650	6.1
Performance ratio PR	3.44	--	--

Figure captions

Fig.1 MED-MVC desalination system diagram.

Fig. 2 Temperature-Entropy (T-S) diagram for a MED-MVC system operation.

Fig. 3 Schematic diagram of the three lumps for the i^{th} effect.

Fig. 4 Control volume for preheaters of (a) distillate and (b) brine.

Fig. 5 Procedures of the steady-state and dynamic models solution method.

Fig. 6 Cost flow diagram with exergy destruction for main component of MED-MVC systems.

Fig. 7 Effect of the number of effects on SPC, η_{II} and TWP.

Fig. 8 Brine level, vapor temperature, brine and vapor flow for a 10% reduction in compressor work.

Fig. 9 Brine level, vapor temperature, brine and vapor flow for a 10% increase in inlet seawater temperature.

Fig. 10 First effect brine level and plant total distillate production with a 15% decrease in inlet seawater temperature for MED-TVC and MED-MVC systems.

Fig. 11 Brine level, and vapor temperature with intensity of reduction in: (a) compressor work, (b) inlet seawater temperature.

Fig. 12 Effect of step changes of compressor work and seawater temperature on the MED-MVC total distillate production, PR and SPC.

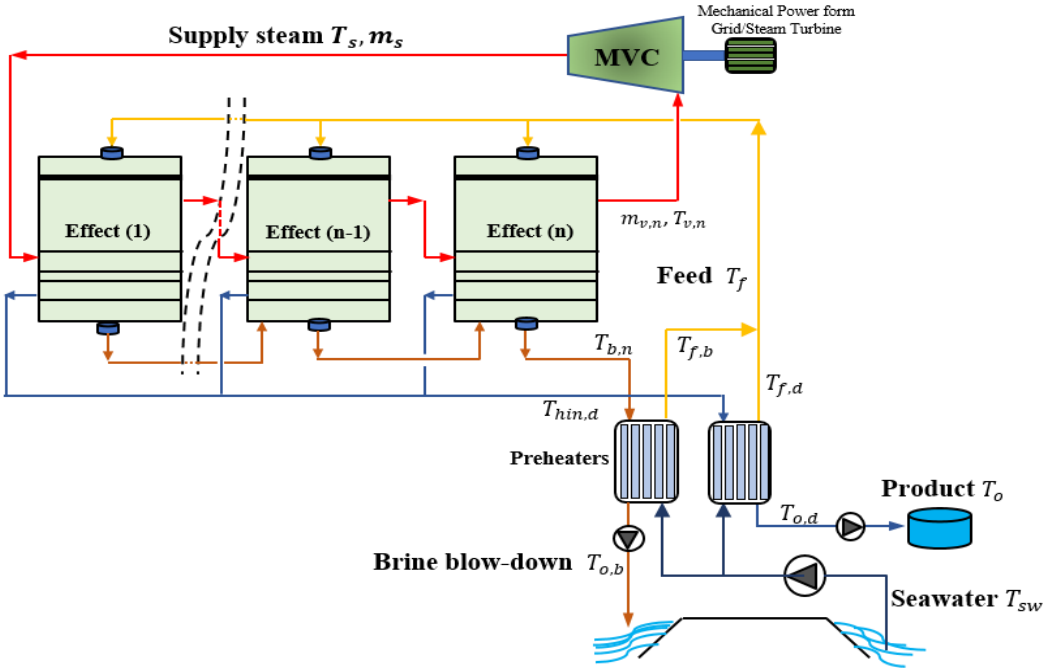

Fig. 1 MED-MVC desalination system diagram.

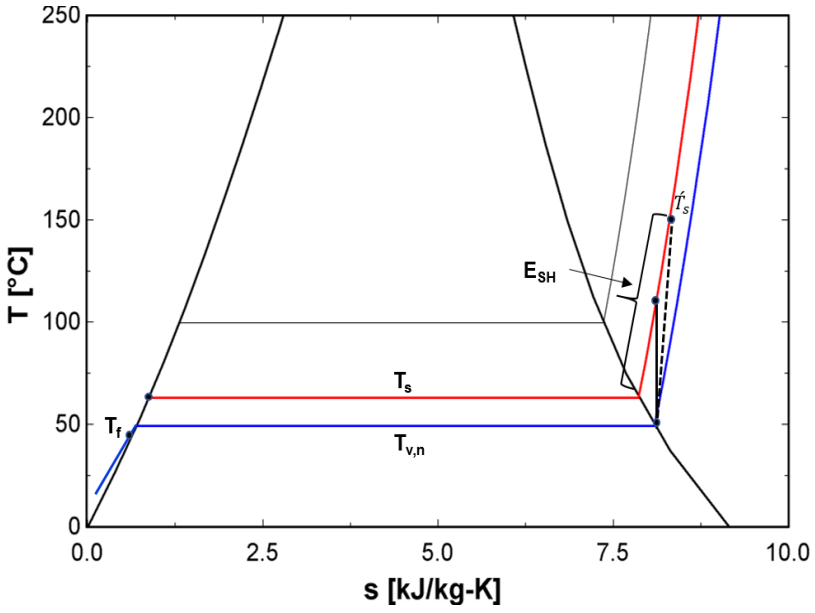

Fig. 2 Temperature-Entropy (T-S) diagram for a MED-MVC system operation.

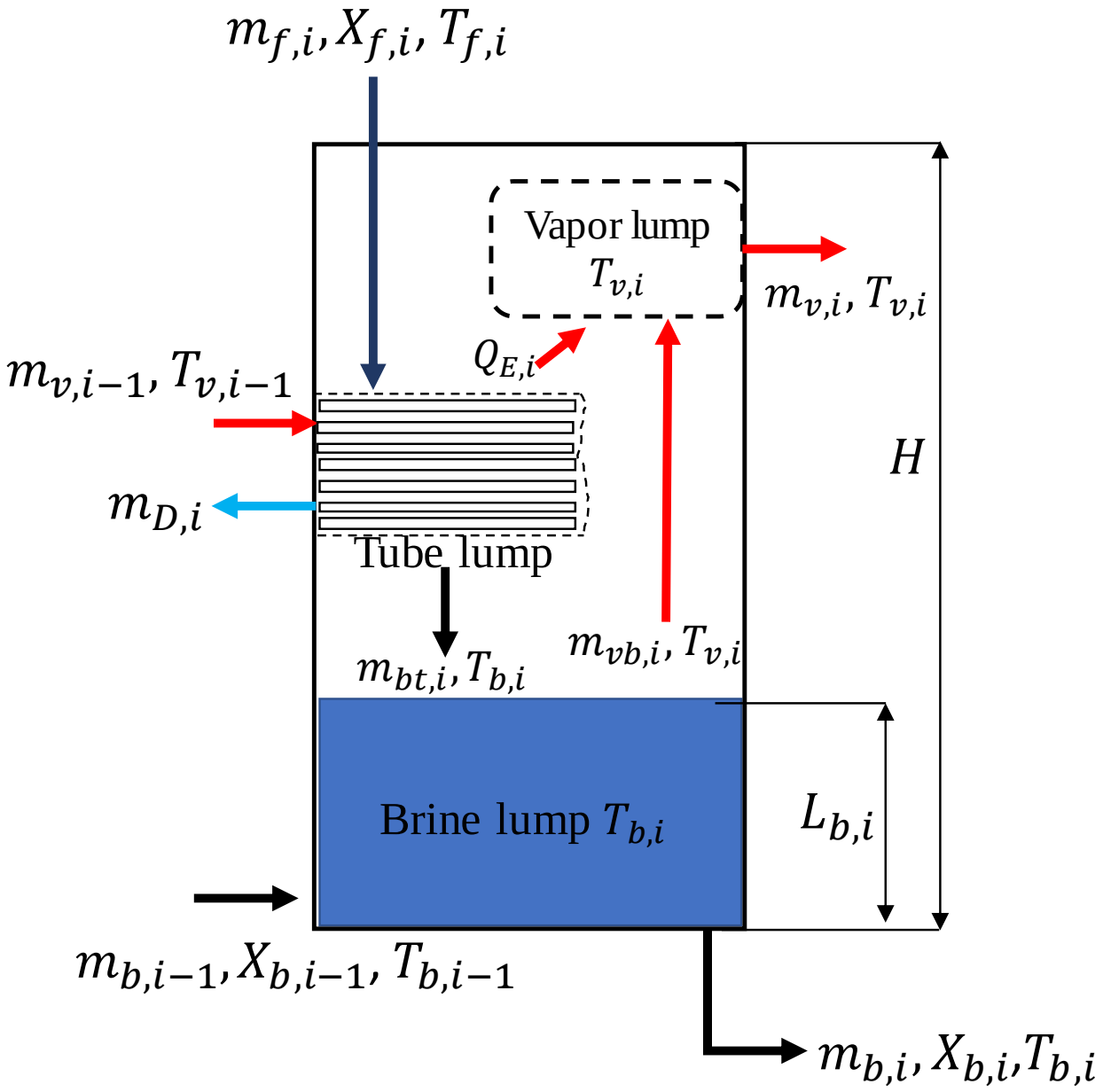

Fig. 3 Schematic diagram of the three lumps for the ith effect.

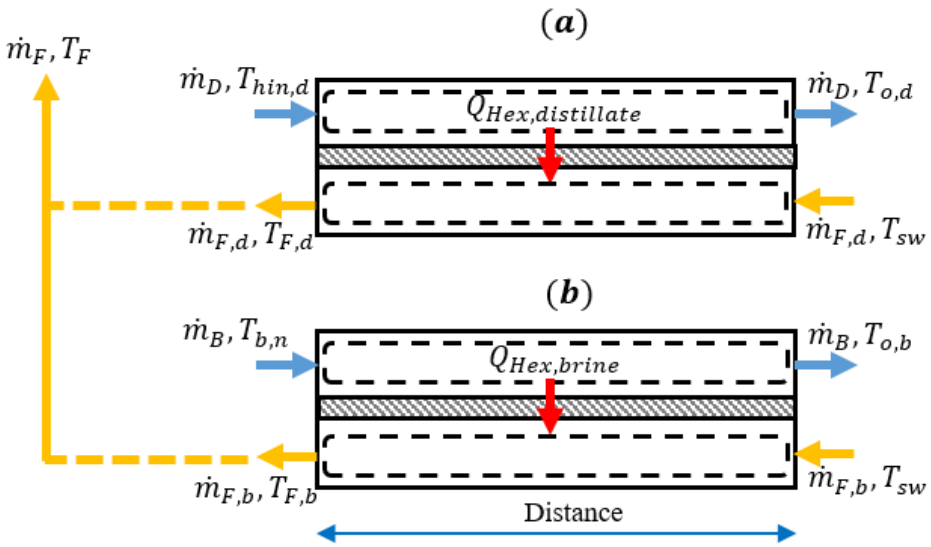

Fig. 4 Control volume for preheaters of (a) distillate and (b) brine.

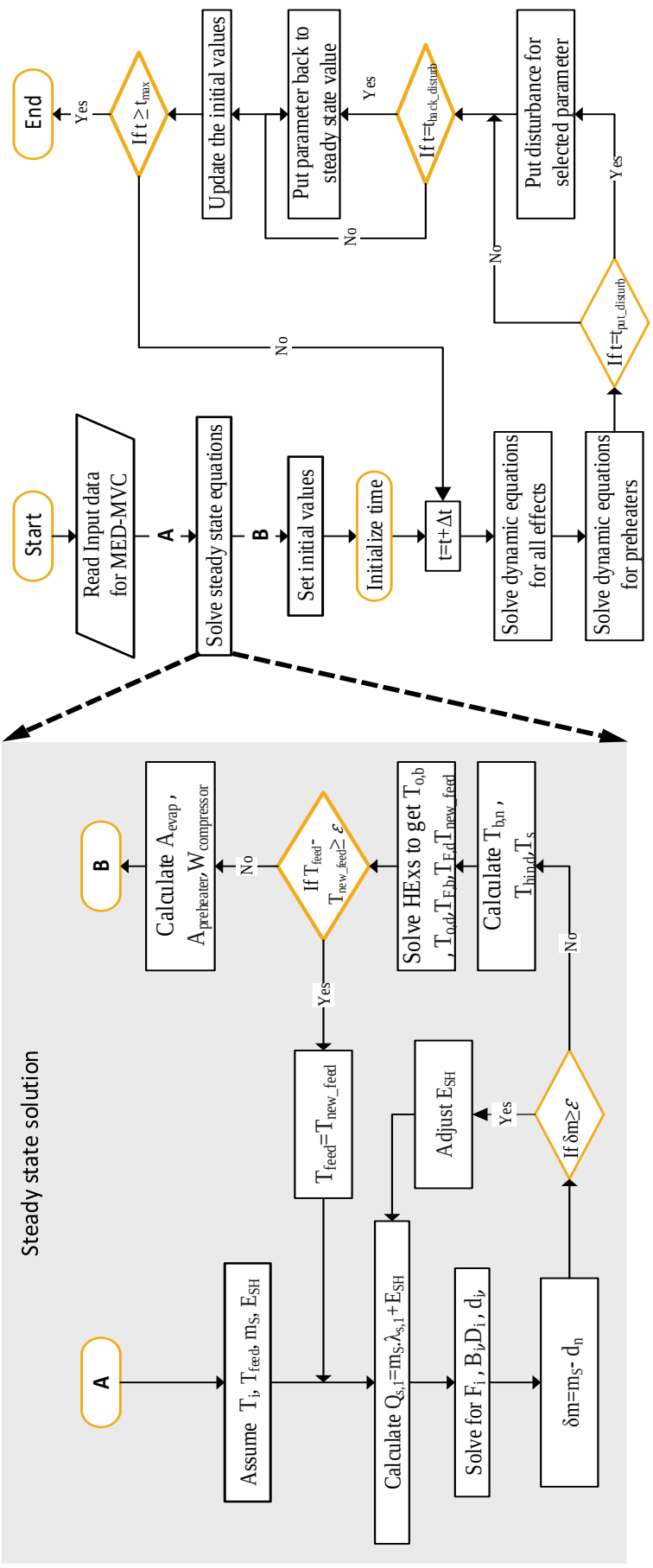

Fig. 5 Procedures of the steady-state and dynamic models solution method.

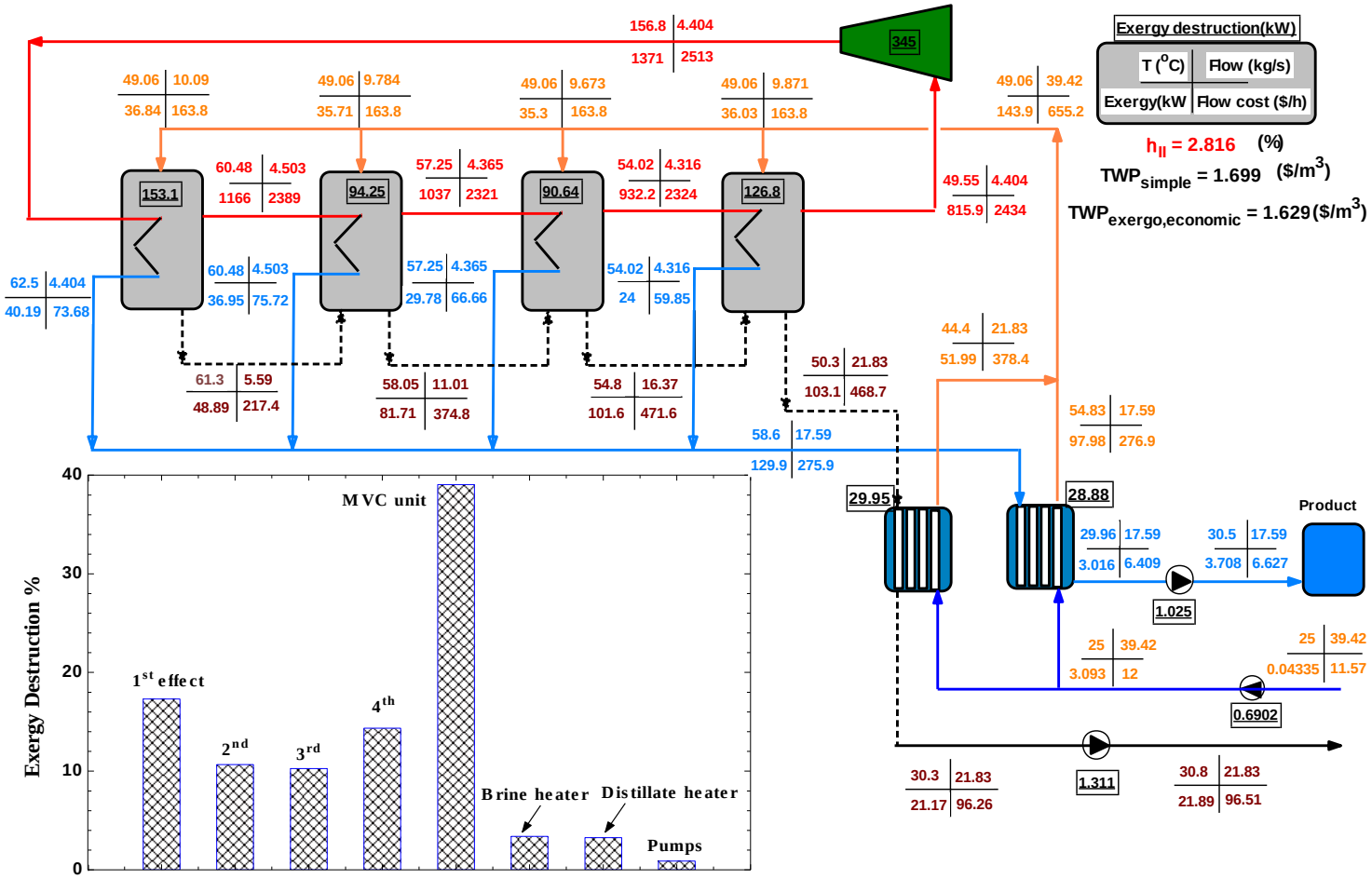

Fig. 6 Cost flow diagram with exergy destruction for main component of MED-MVC systems.

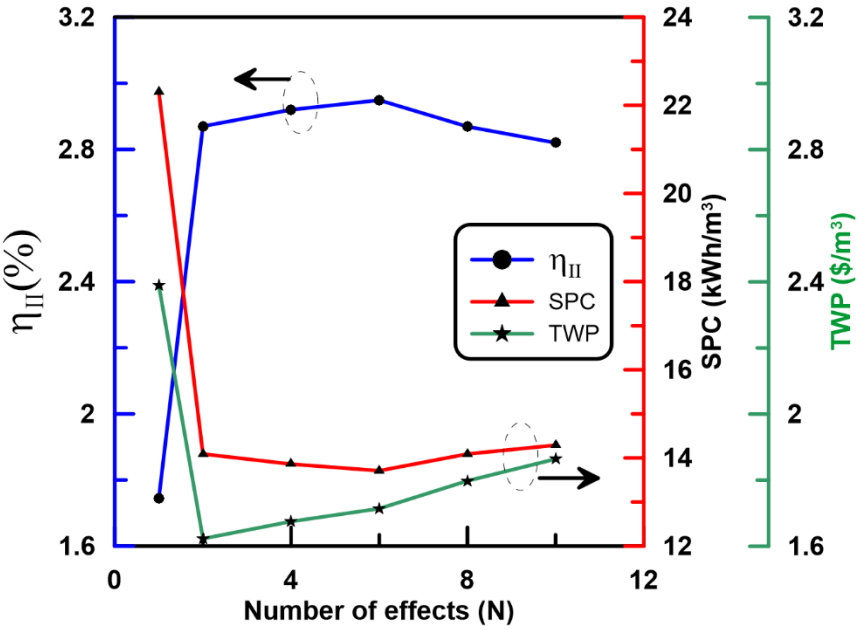

Fig. 7 Effect of the number of effects on SPC, η_{II} and TWP.

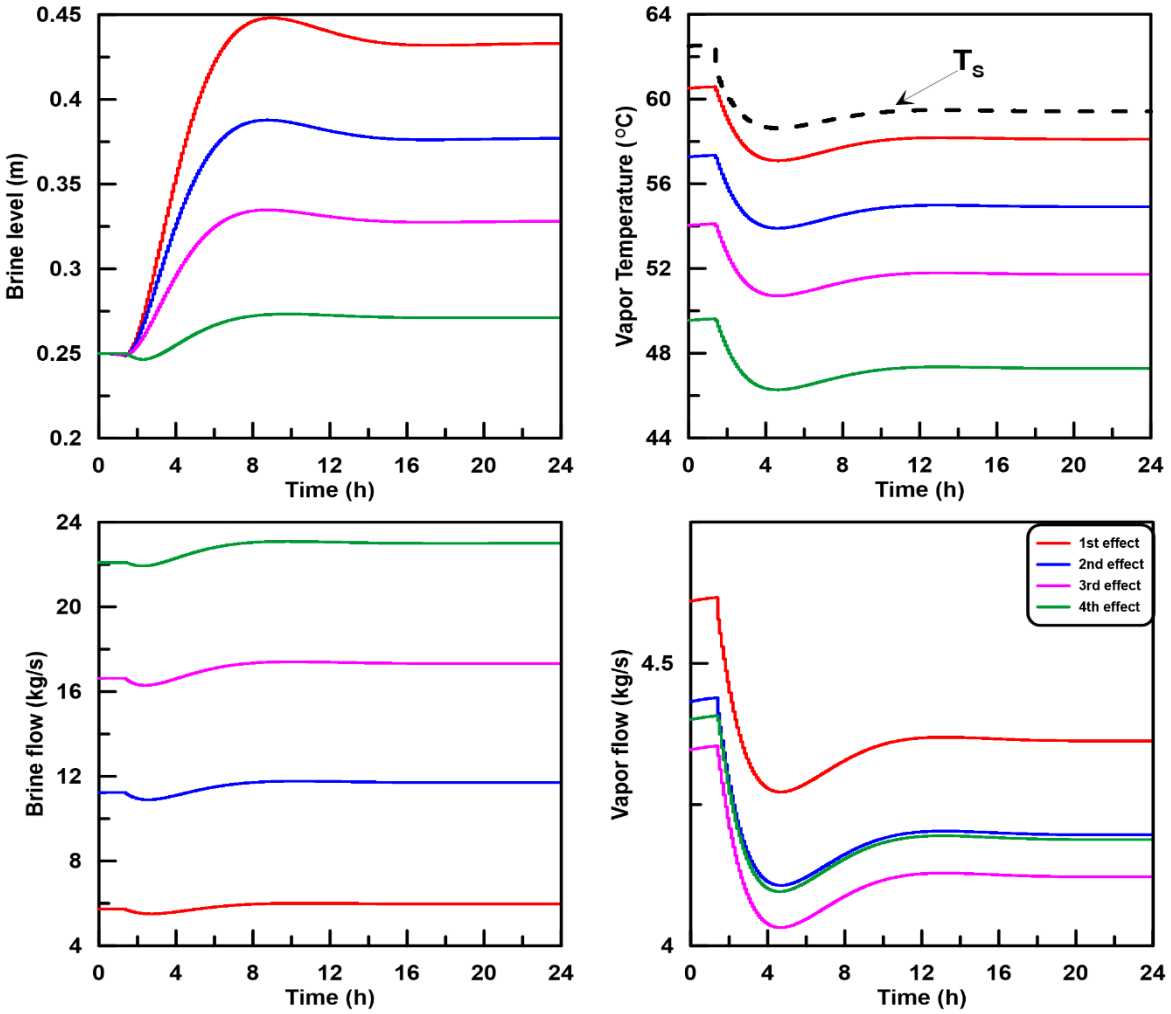

Fig. 8 Brine level, vapor temperature, brine and vapor flow for a 10% reduction in compressor work.

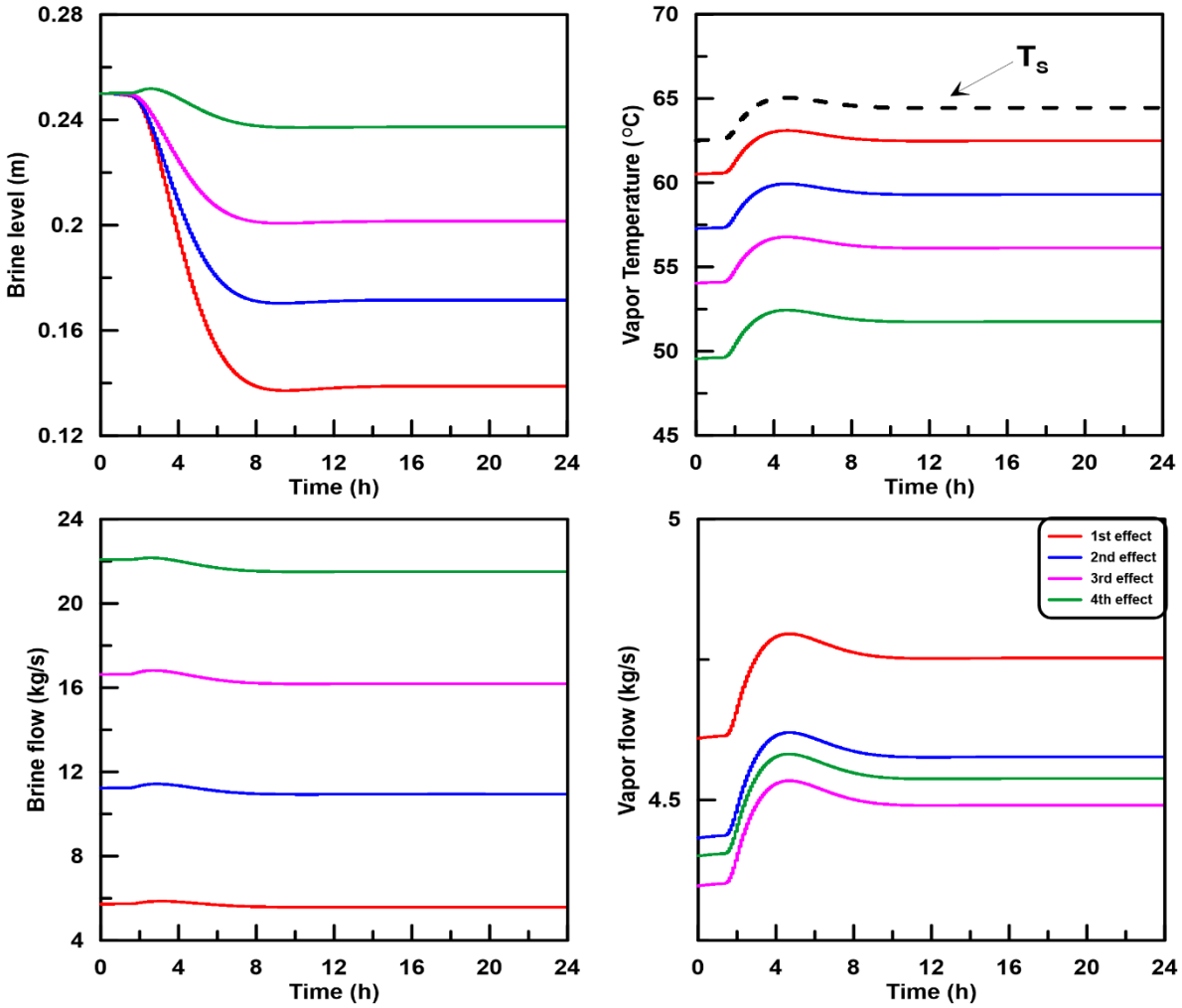

Fig. 9 Brine level, vapor temperature, brine and vapor flow for a 10% increase in inlet seawater temperature.

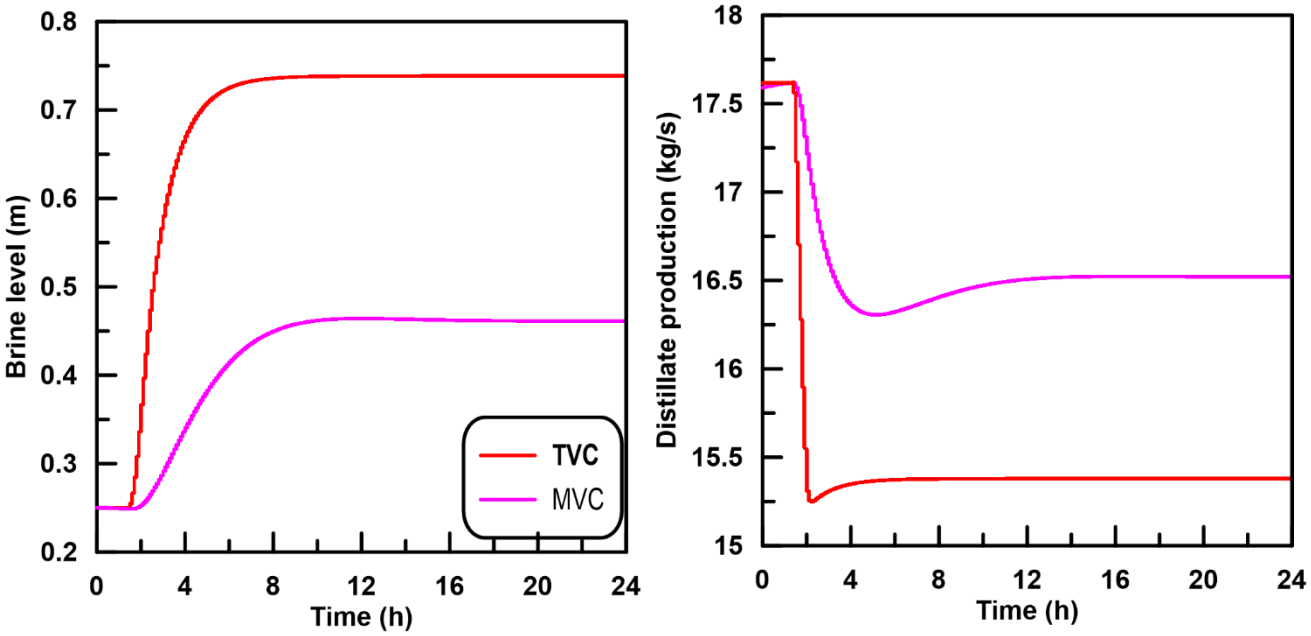

Fig. 10 First effect brine level and plant total distillate production with a 15% decrease in the inlet seawater temperature for MED-TVC and MED-MVC systems.

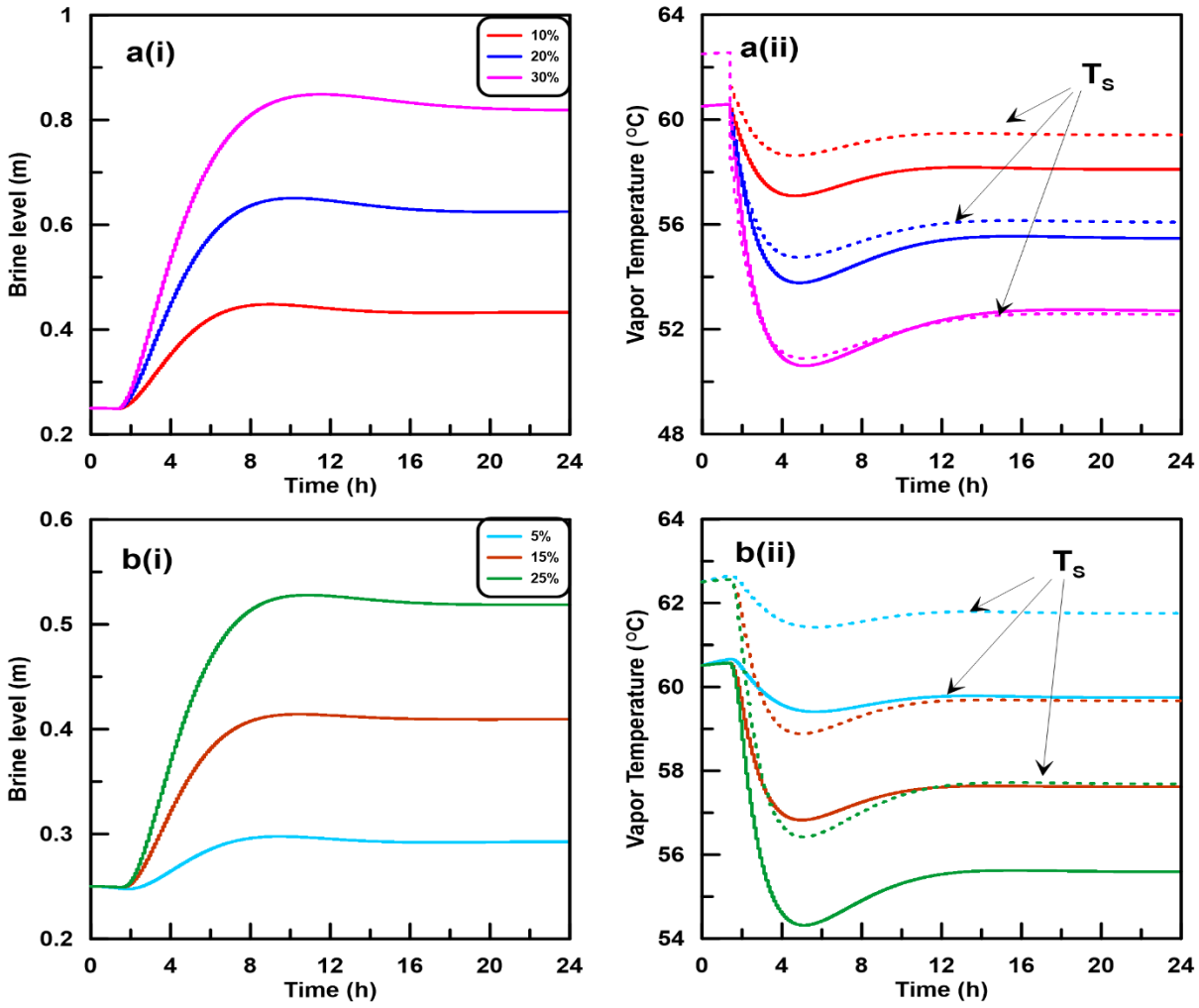

Fig. 11 First effect brine level, and vapor temperature with intensity of reduction in: (a) compressor work, (b) inlet seawater temperature.

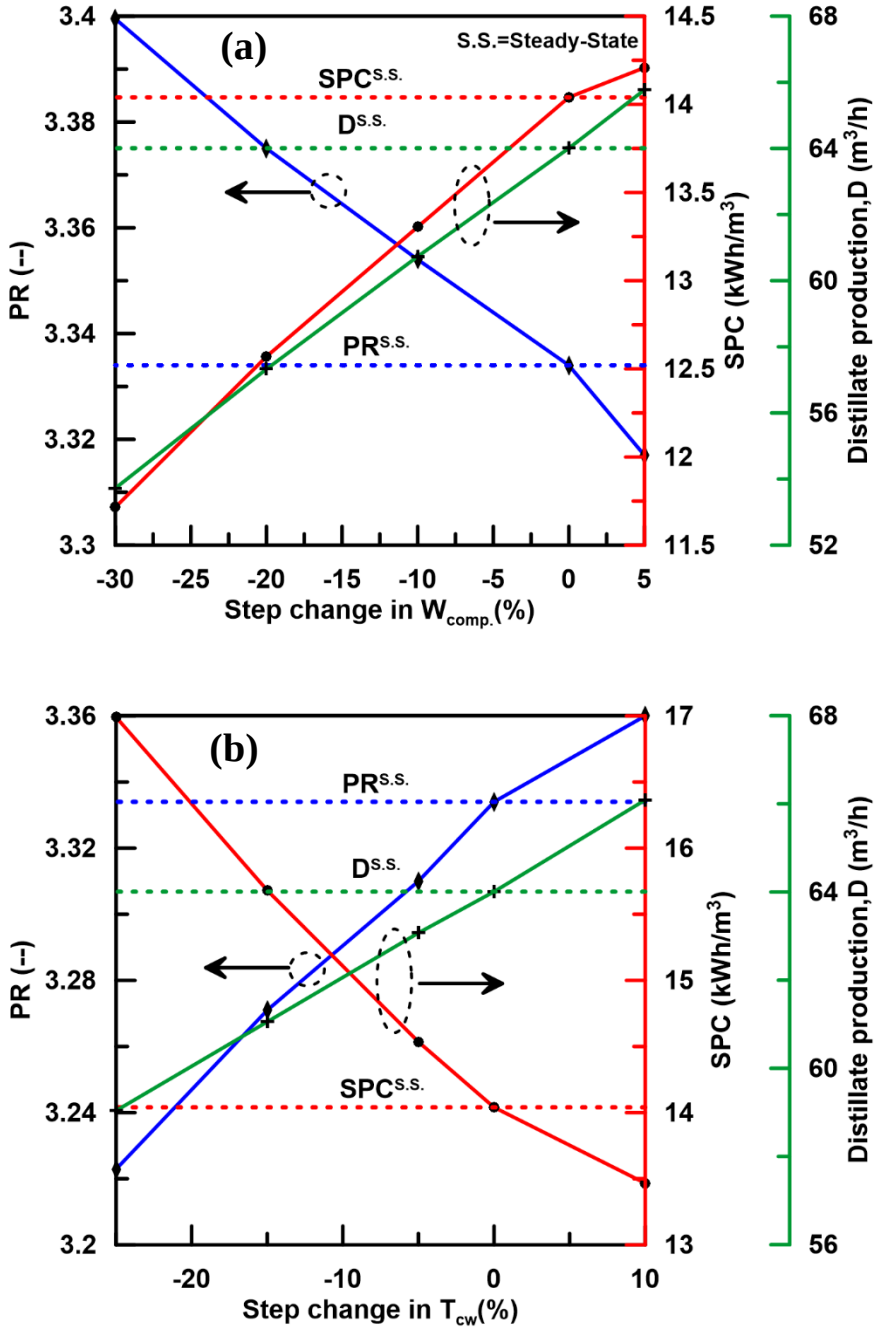

Fig. 12 Effect of step changes of compressor work and seawater temperature on the MED-MVC total distillate production, PR and SPC.